1972

Specification of marine surface boundary layer parameters.

McConathy, Donald Reed.

Monterey, California. Naval Postgraduate School

NAVAL POSTGRADUATE SCHOOL
Monterey, California

THESIS

SPECIFICATION OF MARINE SURFACE

BOUNDARY LAYER PARAMETERS

by

Donald Reed McConathy, Jr.

Thesis Advisor: Kenneth L. Davidson

March 1972

Approved for public release; distribution unlimited.

NAVAL POSTGRADUATE SCHOOL
Monterey, California

THESIS

SPECIFICATION OF MARINE SURFACE

BOUNDARY LAYER PARAMETERS

by

Donald Reed McConathy, Jr.

Thesis Advisor: Kenneth L. Davidson

March 1972

Specification of Marine Surface Boundary Layer Parameters

by

Donald Reed McConathy, Jr.
Lieutenant, United States Navy
B.S., Pennsylvania State University, 1965

Submitted in partial fulfillment of the
requirements for the degree of

MASTER OF SCIENCE IN METEOROLOGY

from the

NAVAL POSTGRADUATE SCHOOL

ABSTRACT

Specification of parameters defining the mean, as well as the turbulent properties, of the over water surface layer is examined. A baroclinic boundary layer model is considered using Cardone's modifications for the marine environment.

Data fields of pressure and temperature were selected as input, and original ship observations were utilized to verify the predicted surface parameters. The effects of stability changes, isobaric curvature, thermal wind, and the value of the von Kármán constant in the model were examined with results shown.

Iteration criteria used in the model were evaluated with respect to operational application. Winds calculated by the model at the height of 19.5 meters were incorporated into the current FNWC wave height program, and the results compared with observed wave data. Turbulent parameters describing the properties of the index of refraction (C_n^2) were also computed and evaluated with respect to laser propagation criteria.

TABLE OF CONTENTS

LIST OF FIGURES

TABLE OF SYMBOLS

a_h	Reciprocal of the turbulent Prandtl number (K_H/K_m)
B	Boston constant = 0.81
B_o	Blackadar constant = 0.0003
C_n^2	Refractive index structure constant
C_p	Specific heat of air at constant pressure
C_T^2	Structure constant for temperature fluctuations
C_z	Nondimensional drag coefficient at level z
ε	Rate of dissipation of turbulent energy
η	Angle between the geostrophic wind and the thermal wind
f	Coriolis parameter
G	Surface geostrophic wind speed
g	Gravity = 9.8 meters/second
H	Upward turbulent heat flux
h	Height of surface layer
K	Streamwise component of wave number
K_c	Curvature
K_H	Turbulent transfer coefficient for heat
K_m	Turbulent transfer coefficient for momentum
k	von Kármán constant
L	Lettau - Monin - Obukhov stability length
L'	Modified stability length

L_*	Dimensionless stability length
N	Measure of the "smearing" of temperature inhomogeneities
ν	Kinematic viscosity
p, q, s	Baroclinic model parameters
p'	Dimensionless baroclinic model parameter
P	Surface pressure (millibars)
ϕ_D	Divergence terms
ϕ_t	Nondimensional temperature gradient
ϕ_θ	One-dimensional spectrum for temperature fluctuation
ϕ_u	Nondimensional wind shear
Ψ	Integrated profile stability parameter
Ψ_o	Surface geostrophic wind angle
R	Radius of curvature
R_d	Gas constant for dry air
R_i	Richardson number
$\bar{\rho}_a$	Mean density of surface boundary layer
r	Dimensionless thermal wind
T_a	Surface air temperature (°C)
T_s	Sea surface temperature (°C)
θ	Potential temperature (°K)
θ_*	Scaling temperature
θ_a	Air temperature measured at level of thermometer (°K)

θ_o	Potential temperature at the surface (°K)
θ_s	Sea surface temperature (°K)
τ	Surface stress
U_*	Friction velocity
U_h	Wind at level h
U_o	Surface wind
U_z	Wind at height z
u_g, v_g	u, v components of geostrophic wind
u_T, v_T	u, v components of thermal wind
V_G	Gradient wind
W	Ageostrophic wind component
W_A	Wave height (feet)
z	Height above sea level (meters)
z_o	Surface roughness parameter (meters)

ACKNOWLEDGEMENT

This research was conducted under the advice of Professor Kenneth Davidson, Department of Meteorology, with considerable assistance from Dr. Jack Kaitala of the Fleet Numerical Weather Central. Professor R. E. Elsberry reviewed the final manuscript.

The project required utilization of the Computer Facility of the Naval Postgraduate School and environmental data from the Fleet Numerical Weather Central in Monterey, National Weather Records Center in Asheville, N. C., and from participating units in the PARKA II experiment conducted in the Pacific in 1969.

I would like to express my sincere thanks to my advisors and members of the above facilities and units, without whose help the study could not have been completed. Especially, I want to thank my wife, Evelyn, for her patience and understanding during this study and also for her typing and proofreading of the manuscript.

I. INTRODUCTION

Parameterization of the boundary layer over the sea surface has been receiving increased attention in recent years. Fortunately much of the theory developed for low level turbulence over a land surface is also applicable over the oceans. But the air-water interface does present some unique problems. For instance a fluid surface, rather than a fixed one, results in mobile surface roughness elements. Because of the presence of a fluid surface, any parameterization requires a knowledge of the processes which transfer heat and momentum energy across the boundary and ultimately influence such variables as wave generation and index of refraction.

The purpose of this study was to examine and evaluate several features of a recently formulated marine boundary layer model which was designed for operational use. The model is a two-layer baroclinic model for the marine boundary layer and the formulation examined was that developed by Cardone (1969). Cardone based his formulation on an earlier two-layer model due to Blackadar (1965a). Features of interest in the model are related to the physics of the planetary boundary layer and include the effect of atmospheric stability, baroclinicity, coriolis acceleration and changes in the surface roughness parameter on the pressure driven surface wind.

The scope of the study was to examine the model in the context of its operational usage. As such, it was a case study in which the data represented pressure and temperature observations from sequential 12-hour periods when a large cyclonic pressure system dominated the Central North Pacific Ocean. This particular synoptic situation provided the necessary relations between the scalar fields to examine features associated with baroclinicity, stability and wind speed categories.

Because these data represent scalar fields which had to be defined by some analysis scheme before being used as input to the two-layer model, the differences which arise due to procedures in the external field specifications are considered. The effect of isobaric curvature on the surface wind fields is examined and this effect is compared to the changes associated with the physics in the model. The differences which may arise solely because the fields are defined by an objective versus a subjective analysis are considered.

Finally, expressions describing the boundary layer are, by their very nature, empirical. As such, they contain empirical constants and the von Kármán constant (k) is one whose value has recently been questioned. The importance of a suggested change from k=0.40 to 0.35 was considered.

II. ASPECTS OF A PLANETARY BOUNDARY LAYER

A. SURFACE BOUNDARY LAYER

1. Basic Structure of the Boundary Layer

Recent advances in the study of atmospheric turbulence have led to a greater confidence in describing the distribution of wind and temperature in the atmospheric boundary layer over a solid surface. This progress has arisen largely through the application of the Monin-Obukhov similarity theory which has been supported by recent observational studies. Cardone's contribution was primarily to extend Blackadar's two-layer neutral baroclinic boundary layer model over fixed terrain, and then to apply this model to the boundary layer over a fluid surface. The major difference between these boundaries is that the sea surface changes its character as the wind blows over it.

In general, Blackadar's model treats the boundary layer as being formed by both turbulent friction and the coriolis acceleration. All processes are considered to be three dimensional, and the layer is characterized by a density stratification. It is conveniently separated into the three regions depicted in Figure 1. In this delineation the important consideration is the specification of K_m which is the turbulent transfer coefficient for momentum.

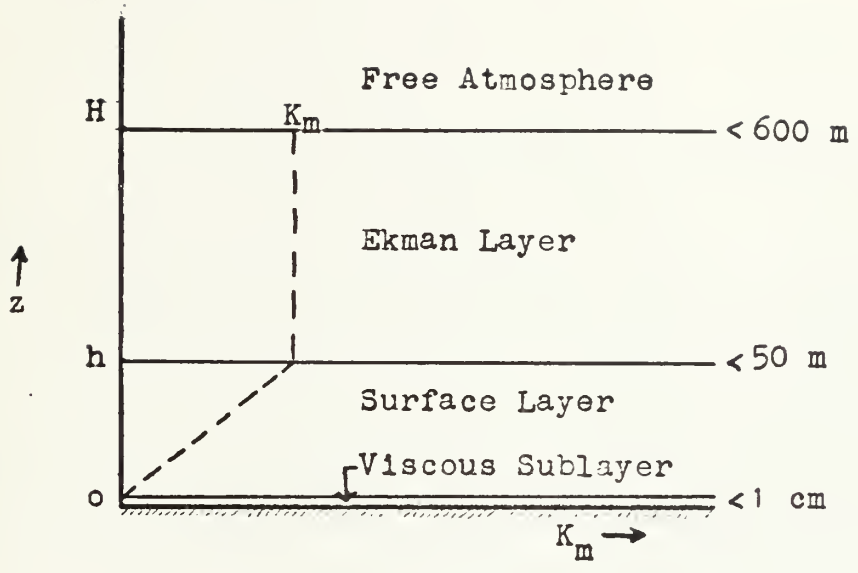

Fig. 1. Diagram of the planetary boundary layer

a. Viscous Sublayer (less than 1 cm)

In this near surface layer the stress is supported by viscosity (aerodynamically smooth flow), and the mean velocity increases linearly according to

$$\overline{U}_z = \frac{U_*^2 z}{\nu} \tag{1}$$

where ν is the kinematic viscosity and U_* is the friction velocity.

b. Surface Layer (up to 50 meters)

This is the constant stress layer in which the coriolis parameter can be neglected and K_m increases linearly with height. For neutral stratification the logarithmic law is valid

$$\overline{U}_z = \frac{U_*}{k} \log {}^{z}/_{z_o} \qquad (2)$$

where k=0.4 is the von Kármán constant.

c. Ekman Layer (50-600 meters)

This layer is characterized by the stress decreasing with height and K_m constant throughout the layer.

In formulating the boundary layer model, Cardone (1969) considered the validity of the "log law" for the surface layer over water, which has been experimentally documented down to near surface limits (Phillips, 1966; Paulson, 1967). He also assumed that the process of wave generation did not seriously affect the surface layer since under neutral and steady conditions a logarithmic shear zone should be established. Accepting the log profile as being valid, Cardone was able to apply much of the surface layer turbulence theory developed over land to over-water conditions. However Cardone did take into account the action of the waves when specifying the effective roughness parameter for the sea surface.

2. Similarity Theory for the Surface Layer

The Monin-Obukhov "similarity theory" has led to considerable progress in the specification of the distribution of wind and temperature in the boundary layer. The basis of this theory is that near the ground there exist velocity (U_*), length (L), and temperature (θ_*) scales which are essentially invariant with height. When the principle variables such as temperature (T), wind (U), and height (z) are expressed

as nondimensional fractions of these quantities, a series of nondimensional equations can be formed which are of general validity in the surface boundary layer (Lumley and Panofsky, 1964). Recent analyses of the oceanic wind data (e.g. Phelps and Pond, 1971) have indicated that the Monin-Obukhov theory is valid for over-water application. These results support Cardone's inclusion of the Monin-Obukhov stability criteria in the boundary layer model.

Similarity theory predicts that a universal relation should exist for the nondimensional wind shear

$$\frac{kz}{U_*} \quad \frac{\partial U}{\partial z} = \phi_u \tag{3}$$

and the nondimensional temperature gradient

$$\frac{z}{\theta_*} \quad \frac{\partial \theta}{\partial z} = \phi_t \tag{4}$$

where ϕ_t and ϕ_u are functions of the dimensionless ratio z/L. Here θ is the potential temperature, θ_* is the scaling temperature defined by

$$\theta_* = -\frac{1}{kU_*} \quad \frac{H}{Cp \quad \overline{\rho}_a} \tag{5}$$

and L is the Lettau-Monin-Obukhov stability length defined by

$$L = \frac{-U_*^3 \; Cp \; \overline{\rho}_a \, T}{k g H} \; . \tag{6}$$

The heat flux (H) is not easily measured, so a modified stability length was defined by Panofsky (1963)

$$L' = a_h L = \frac{K_H}{K_m} L = \frac{U_* T \; \partial u/\partial z}{k g \; \partial\theta/\partial z} \; . \tag{7}$$

The assumption that L' is independent of height implies that a_h is constant, which in turn implies similarity between wind and temperature profiles.

If L' is a valid scaling length, similarity theory predicts that

$$\frac{kz}{U_*} \frac{\partial U}{\partial z} = \phi_u (z/L') \tag{8}$$

$$\frac{z}{\theta_*} \frac{\partial \theta}{\partial z} = \frac{\phi_u (z/L')}{a_h} . \tag{9}$$

Integration of these formulae (Panofsky, 1963) yields

$$U_z = \frac{U_*}{k} \left[\ln z/z_o - \Psi(z/L') \right] \tag{10}$$

$$\theta_z = \theta_o + \frac{\theta_*}{a_h} \left[\ln z/z_o - \Psi(z/L') \right] , \tag{11}$$

where the relation between Ψ and ϕ_u is

$$\Psi(z/L') = \int_o^{z/L'} \frac{1 - \phi_u(\xi)}{\xi} d\xi , \quad \xi = z/L' . \tag{12}$$

Paulson (1970), using the KEYPS formula, integrated (12) by parts to obtain the following expression for Ψ

$$\Psi = 1 - \phi_u - 3 \ln \phi_u + 2 \ln \left(\frac{1+\phi_u}{2}\right) + 2 \tan^{-1} \phi_u - \frac{\Pi}{2} + \ln \left(\frac{1+\phi_u^2}{2}\right) . \tag{13}$$

Within the scope of an operational application, these expressions for the surface layer would be used to determine the wind speed given U_*, or to determine U_* given the wind speed at a particular level. For this reason the partial derivatives in (7) are replaced by expressions involving height differences and air-sea temperature

differences. This is achieved by substituting the following expression for $\frac{\partial \theta}{\partial z}$, obtained by combining (9) and (11)

$$\frac{\partial \theta}{\partial z} = \frac{\phi_u \left(\frac{z_a}{L'}\right)(\theta_a - \theta_s)}{z\left[\ln\left(z_a/z_o\right) - \Psi\left(z_a/L'\right)\right]}, \qquad (14)$$

where z_a is the height at which θ_a is measured (chosen as 10 meters by Cardone).

Substituting (14) and (8) into (7) yields

$$L' = \frac{U_*^2 \bar{\theta}\left[\ln\left(\frac{z_a}{z_o}\right) - \Psi\left(z_a/L'\right)\right]}{k^2 g\left(\theta_a - \theta_s\right)}. \qquad (15)$$

Equation (10) is then solved for U_*

$$U_* = \frac{k\, U_m}{\ln\left(z_m/z_o\right) - \Psi\left(z_m/L'\right)}, \qquad (16)$$

where z_m is the height at which the wind speed is measured (chosen as 19.5 meters by Cardone). Equations (15) and (16) can then be solved for U_* given the wind speed at some level (U_z) and the air-sea temperature difference.

3. Consideration of the Drag Coefficient (C_z) and Roughness Parameter (z_o)

The surface roughness parameter and the influence of thermal stratification have received considerable attention in the definition of the relation between the nondimensional drag coefficient (C_z) and the wind speed at a certain height (usually 10 meters). The need for such a relation arises from the "bulk aerodynamic" formula for estimating

momentum flux. This equation, deduced from dimensional analysis, has the form

$$\tau = \overline{\rho}_a \, U_*^2 = \overline{\rho}_a \, C_z \, U_z^2 \quad , \tag{17}$$

where τ is the surface stress. From this expression the drag coefficient is defined as

$$C_z = \frac{U_*^2}{\overline{U}_z^2} \quad . \tag{18}$$

Rearranging and squaring (10) yields the following expression for the drag coefficient at a level z in terms of z_o and stability

$$C_z = \left[\frac{k}{\ln {}^{z}/z_o - \Psi ({}^{z}/L')} \right]^2 . \tag{19}$$

which was the form considered by Cardone.

Observations have indicated that over the sea, z_o is dependent on U_*. This dependence, however, changes as the wind speed changes. For the case of light winds (aerodynamically smooth flow), the drag coefficient C_z decreases with increasing wind speed (Kraus, 1966) and z_o has the form

$$z_o = \frac{\nu}{1.09 \, U_*} \quad . \tag{20}$$

For aerodynamically rough flow, C_z increases with increasing wind speed according to

$$z_o = \frac{a \, U_*^2}{g} \tag{21}$$

where (a) is a constant = 0.035 (Charnock, 1955). A summary of field

observations indicates that the change between rough and smooth flow occurs at wind speeds of 5-6 meters/second.

Cardone proposed the following simple expression for z_o covering a wide range of wind speeds (both rough and smooth flow)

$$z_o = \frac{C_1}{U_*} + C_2 U_*^2 + C_3 . \qquad (22)$$

The constants were chosen so that C_z was a minimum for a value of 6 meters/second at the 10 meter height under neutral conditions, and above this speed the relation approximated Charnock's results. For U_* in meters/second and z_o in meters, the resulting expression was

$$z_o = 6.84 \times 10^{-5}/U_* + 4.28 \times 10^{-3} U_*^2 - 4.43 \times 10^{-4}. \qquad (23)$$

Other representations of C_z versus U_z have been published. A few of these appear in Figure 2 along with Cardone's approximation. It is clear from the scatter of curves in Figure 2 that the specification of the drag coefficient was a primary decision in Cardone's formulation. This choice of C_z versus U_z will be examined during the discussion on results from this investigation.

With the equations for stability length (15), friction velocity (16), and surface roughness parameter (23), the surface layer wind distribution is completely described within the framework of the similarity theory. These three equations can be solved simultaneously for U_* using iteration techniques with the external parameters described below as input.

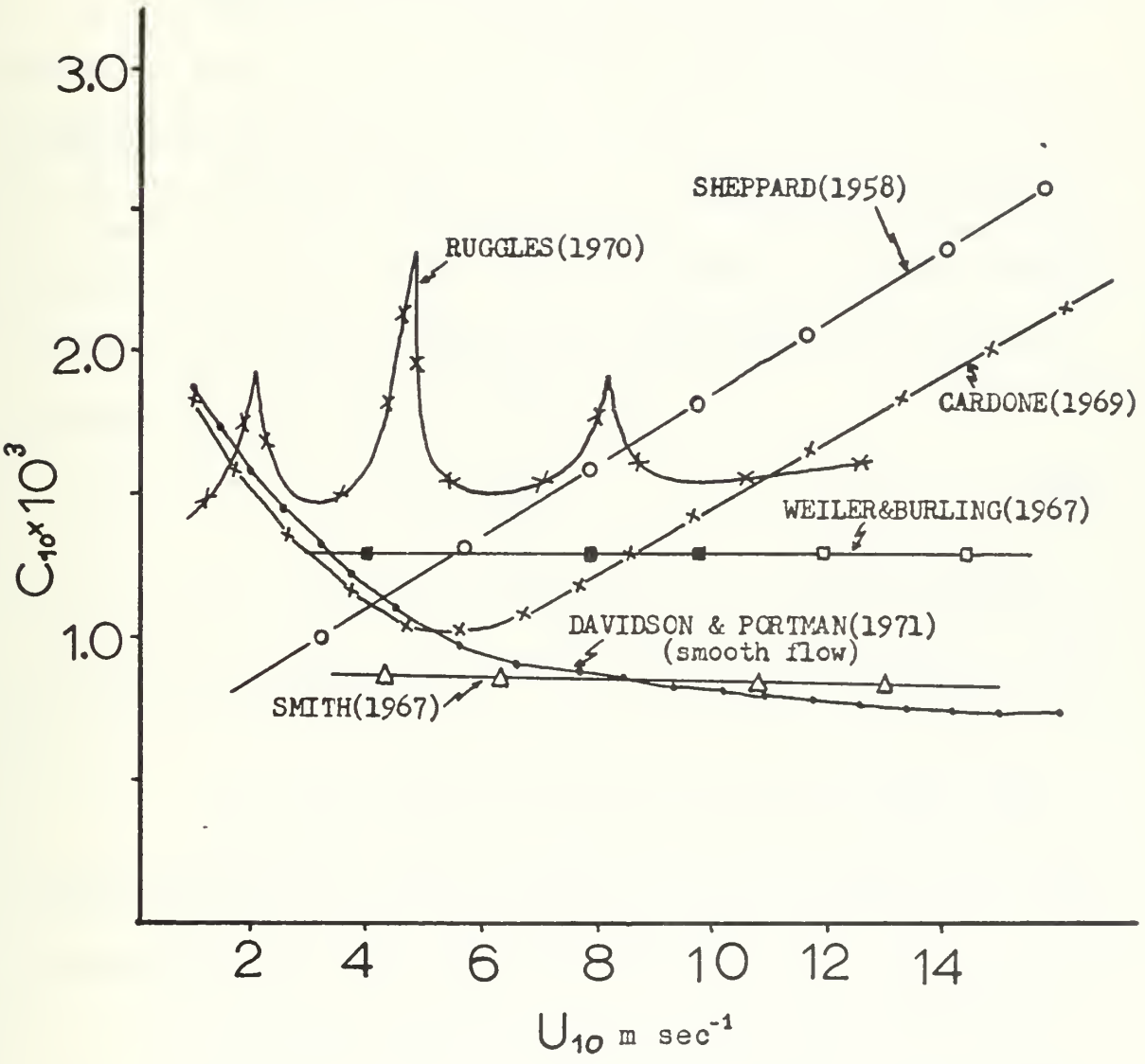

Fig. 2. Various suggested forms of the drag coefficient (C_z) versus windspeed (U_z) at 10 meters

B. PLANETARY BOUNDARY LAYER

1. Background

In developing a model for the entire boundary layer, consideration has to be given to the possible external parameters. In Cardone's formulation these parameters were the geostrophic wind (G), the air-sea temperature difference $(\theta_a - \theta_s)$, the coriolis parameter (f), and the thermal wind (r). He considered previously suggested empirical relations between the geostrophic drag coefficient (U_*/G) and the surface Rossby number (Lettau, 1959)

$$R_o = \frac{G}{f z_o} \quad , \tag{24}$$

where G is the surface geostrophic wind speed. Empirical relations have also been suggested between the cross isobar flow angle Ψ_o and R_o.

Blackadar (1965a) developed a two-layer boundary layer model, consisting of a Prandtl surface layer and an Ekman layer, which was verified on the basis of the above relations.

Cardone's formulation was closely related to Blackadar's work. In particular, the height of the surface layer (h) was specified explicitly in terms of the external parameters

$$h = \frac{B_o G}{f} \tag{25}$$

where B_o was a nondimensional constant equal to 3.0×10^{-4} as determined by Blackadar.

By applying proper boundary conditions and requiring that continuity of wind and wind shear exist at level h, the following solutions for U_*/G and Ψ_o (along with the solution for z_o) completely define the surface boundary layer wind distribution under neutral conditions.

$$\frac{U_*}{G} = \left[2\ k\ B_o \sin^2\ \Psi_o \right]^{3/2} \tag{26}$$

$$\frac{U_*}{G} = \frac{k\sqrt{2}\ \sin\ (\pi/4 - \Psi_o)}{\ln B_o R_o} \tag{27}$$

Implicit in such an approach is that the value of K_m at the internal boundary between the surface layer and the Ekman layer is given by

$$K_m = \frac{k U_* G}{f} . \tag{28}$$

2. Cardone's Extension of Blackadar's Two-Layer Model

The success of Blackadar's two-layer model in predicting the essential characteristics of the neutral surface boundary layer, along with its relative ease of application, suggested its extension to the non-neutral marine boundary layer. Cardone extended the diabatic model to over-water flow by regarding z_o as a function of U_*.

The eddy viscosity in the constant stress layer for the non-neutral case was expressed by Cardone in terms of the nondimensional wind shear as

$$K_m = \frac{k U_* z}{\phi_u (z/L')} . \tag{29}$$

Since K_m is constant with height above h, its value in the Ekman layer is then

$$K_m = \frac{k U_* B_o G}{f \phi_u (z/L')} \quad . \tag{30}$$

The wind speed at h was given by

$$U_h = \frac{U_*}{k} \left[\ln B_o R_o - \Psi (h/L') \right] . \tag{31}$$

Internal boundary conditions applied at level h appear in Figure 3 and follow from the fact that $\frac{\partial W}{\partial z}$ always makes an angle of $\frac{3\Pi}{4}$ to the ageostrophic wind (W) and that $\frac{\partial U}{\partial z}$ is parallel to U in the constant stress layer.

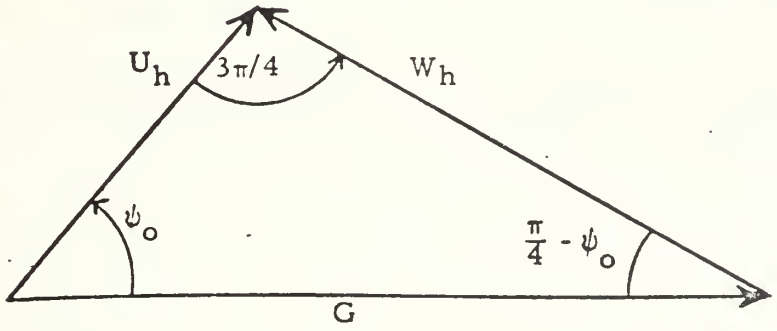

Fig. 3. Wind vector diagram applicable at level h.

By requiring continuity of wind shear at h, as well as directional continuity, Cardone was able to reduce the problem (analogous to (26) and (27)) to

$$\frac{U_*}{G} = \left[2 k B_o \sin^2 \Psi_o \phi_u (h/L') \right]^{1/2} \tag{32}$$

$$\frac{U_*}{G} = \frac{k\sqrt{2} \sin (\Pi/4 - \Psi_o)}{\ln B_o R_o - \Psi (h/L')} \quad . \tag{33}$$

These equations are solved simultaneously for $\frac{U_*}{G}$ and Ψ_o from the external parameters G, f, and $(\theta_a - \theta_s)$. In addition, a dimensionless stability parameter was defined as

$$L_* = \frac{B_o G}{f L'} \tag{34}$$

which represented the ratio of the surface layer h to the stability length L' (Blackadar and Ching, 1965).

The relationships determined by Cardone for U_*/G and Ψ_o as functions of R_o and L_* appear in Figures 4 and 5. For all surface Rossby numbers, U_*/G increases and Ψ_o decreases with decreasing stability. In general, stable conditions have a more pronounced effect on the surface layer wind characteristics than unstable conditions. In comparing the results from the model with observations, Cardone noted that U_*/G increased by roughly 30% in unstable conditions, with no marked tendency to decrease at great instability, and decreased roughly 70% in stable conditions. These features in the observed results will be discussed later.

The effects of baroclinicity were also included by assuming that the geostrophic wind was a linear function of height (Blackadar, 1965b). Blackadar (1965a) introduced a parameter, p, which was defined at level h by

$$p = \frac{U_h}{(\partial U/\partial z)_h} = \frac{B_o G}{f \phi_u (h/L')} \left[\ln B_o R_o - \Psi (h/L') \right]. \tag{35}$$

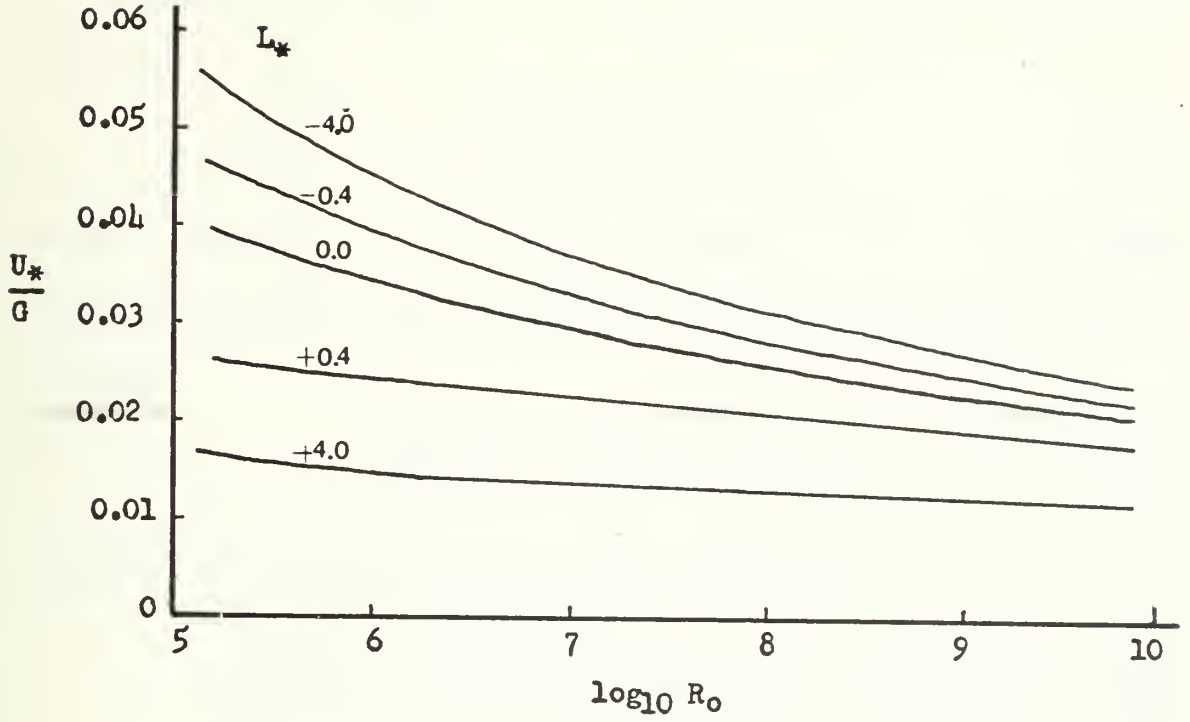

Fig. 4. Variation of the geostrophic drag coefficient with surface Rossby number and dimensionless stability length (L_*) (Cardone, 1969)

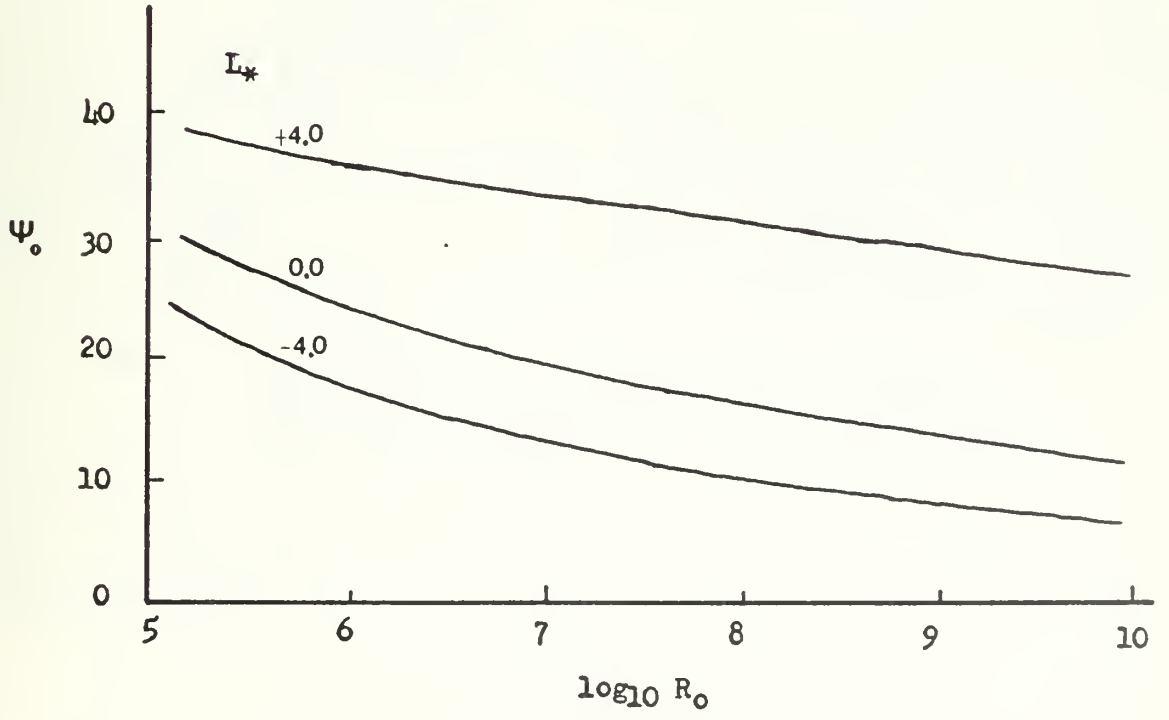

Fig. 5. Variation of surface cross isobar angle with surface Rossby number and stability (Cardone, 1969)

The requirement of continuity of wind shear for the baroclinic case took the form

$$U_h = \bar{p}\left[\left(\frac{\partial G}{\partial z}\right) + \frac{\partial W}{\partial z}\right]_h . \qquad (36)$$

Figure 6 illustrates the geometrical implication of (36). From the Ekman layer solution of the ageostrophic wind, the following equation can be obtained

$$p \left|\frac{\partial W}{\partial z}\right|_h = \sqrt{2}\ p' \ |W_h| , \qquad (37)$$

where p' is a dimensionless parameter defined by

$$p' = \frac{B_o G}{\phi_u (h/L')} \sqrt{\frac{\phi_u (h/L')}{2 k U_* B_o G}} \left[\ln B_o R_o - \Psi (h/L')\right]. \qquad (38)$$

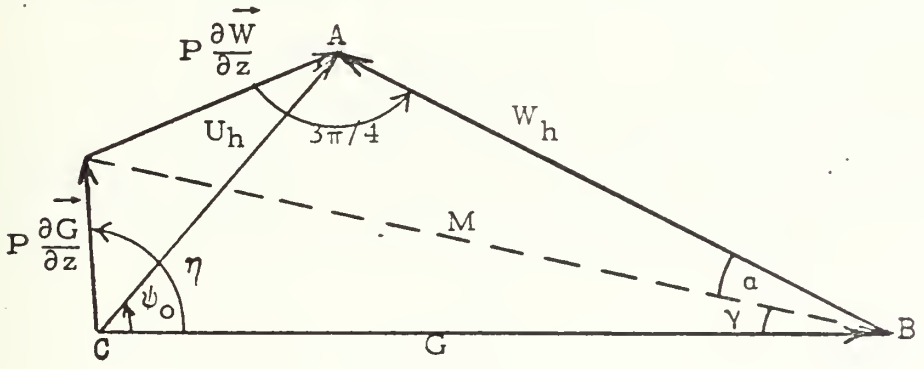

Fig. 6. Geometrical relationships resulting from the requirement of the continuity of wind shear at the internal boundary level h (Blackadar, 1965b).

Next the thermal wind vector was replaced by its dimensionless magnitude

$$r = \frac{1}{f} \left|\frac{\partial G}{\partial z}\right| \qquad (39)$$

where the direction of $\frac{\partial G}{\partial z}$ relative to the surface geostrophic wind was implied by angle η in Figure 6. Still another dimensionless quantity was defined

$$r' = r B_o \left[\ln B_o R_o - \Psi (h/L') \right] \tag{40}$$

and (35) was then rewritten as

$$p \left| \frac{\partial G}{\partial z} \right| = r' G. \tag{41}$$

By applying the law of cosines to each of the two smaller triangles in Figure 6 that have M for one side, the following relations were determined

$$M^2 = \left| W_h \right|^2 s^2 = G^2 q^2 \tag{42}$$

$$s^2 = (1 + 2p' + 2p'^2) \tag{43}$$

$$q^2 = (1 + r'^2 - 2r' \cos \eta). \tag{44}$$

η is the angle between the geostrophic wind and the thermal wind (see Figure 6). Then the law of sines was applied to yield

$$\sin \alpha = p'/s \tag{45}$$

$$\sin \gamma = \frac{r'}{q} \sin \eta \tag{46}$$

The following relations apply to the large triangle (ABC) in Figure 6.

$$U_h = \left| W_h \right| \sin (\alpha + \gamma) / \sin \Psi_o \tag{47}$$

$$U_h^2 = G^2 + \left| W_h \right|^2 - 2G \left| W_h \right| \cos (\alpha + \gamma) \tag{48}$$

$$\left| W_h \right|^2 = U_h^2 + G^2 - 2 U_h G \cos \Psi_o . \tag{49}$$

From equations (31), (45), (46), (47), (48), and (49), the following equations describing the surface boundary layer characteristics were obtained

$$\text{Tan } \Psi_o = \frac{\sin(\alpha + \gamma)}{(s/q) - \cos(\alpha + \gamma)} \tag{50}$$

$$U_* = \frac{k G q \sin(\alpha + \gamma)}{s \sin \Psi_o \left[\ln B_o R_o - \Psi(h/L')\right]} . \tag{51}$$

By including (23) and (15), Cardone obtained a system of equations that could be solved for U_* and Ψ_o from the input parameters G, f, $(\theta_a - \theta_s)$, $\left|\frac{\partial G}{\partial z}\right|$, and η. These equations were calculated from a knowledge of sea level pressure, surface air temperature, sea surface temperature, and latitude.

3. Some Characteristics of the Marine Surface Boundary Layer

A primary effort of Cardone's work was to determine how well the planetary boundary layer model, using only large-scale synoptic parameters as input, specified the surface boundary layer wind distribution over the sea surface. Cardone considered several studies relating the geostrophic wind ratio U_z/G and the air-sea temperature difference. The results of an extensive study by Carstensen (1967) at Fleet Numerical Weather Central (FNWC) appear in Figure 7 along with earlier results due to Bleeker. The ratio of surface wind (V) to geostrophic wind (G) is tabulated for each degree of the reported air-sea temperature difference, and the median value for each interval is plotted as an x in Figure 7. The validity of the results was limited to the air-sea temperature difference range -4 to +1°C. In order to include observed winds in the surface pressure analysis, FNWC uses a constant value for V/G of 0.78 and a turning angle of 15° toward lower pressure. This selection could produce significant error.

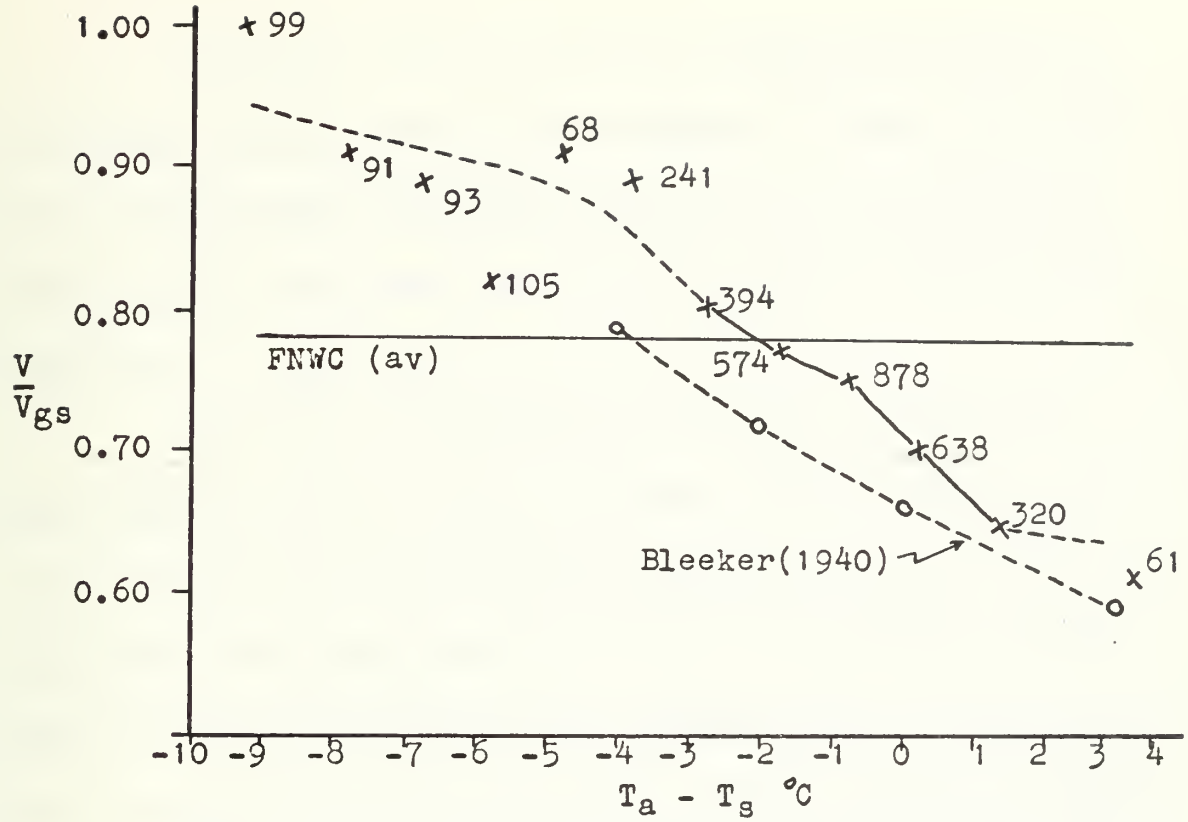

Fig. 7. Reported wind-geostrophic wind ratio as a function of air-sea temperature difference (Carstensen, 1967)

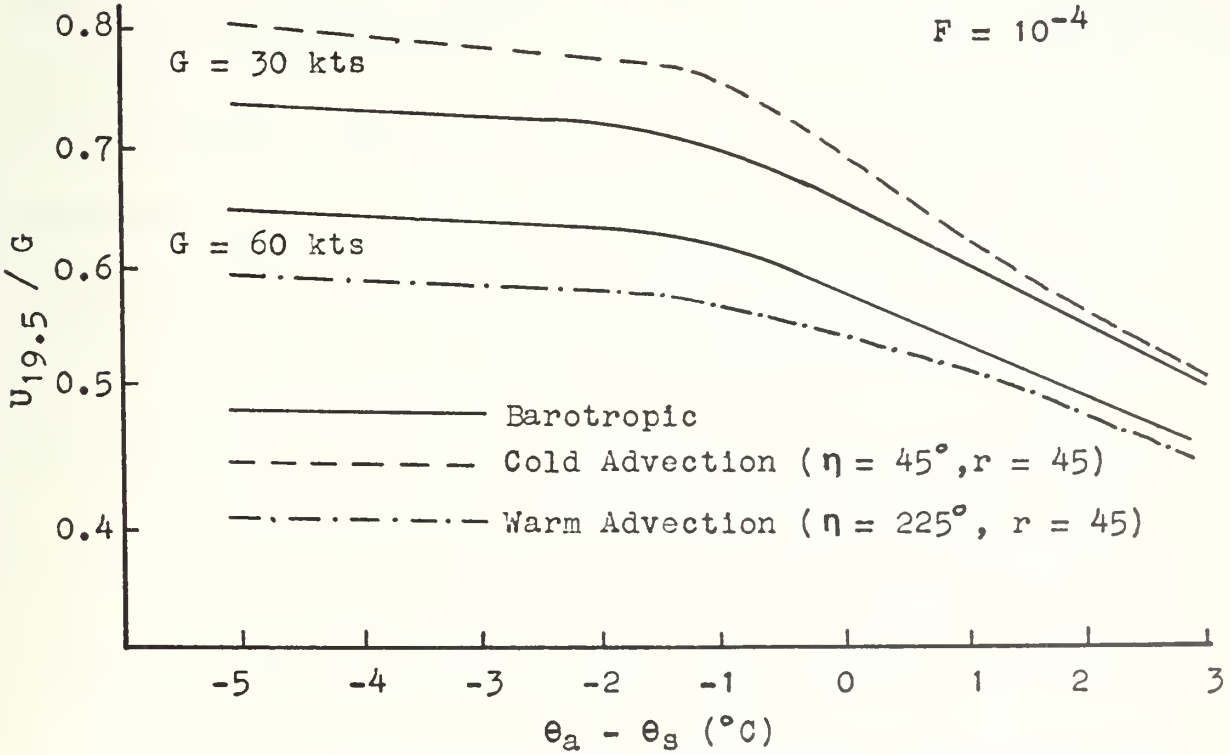

Fig. 8. Two layer model predictions of the dependence of the ratio of the 19.5 meter wind speed to the geostrophic wind speed upon air-sea temperature difference and thermal advection

Cardone's model can be used to compute a wind speed at 19.5 meters. Figure 8 illustrates the variation of the ratio of the 19.5 meter wind and surface geostrophic wind with the air-sea temperature difference. The ratio varied less in unstable conditions than in stable conditions.

The effects of baroclinicity also appear in Figure 8 and these effects increase as stability decreases, with the ratio, $U_{19.5}/G$, increasing with cold advection and decreasing with warm advection. Mendenhall (1967) also studied the influence of baroclinicity and stability on the veering of the wind in the planetary layer. He concluded that over mid-latitude oceans the diurnal variation of frictional veering of the wind with height was negligible, but that lapse rate and baroclinicity were important. Results obtained by Cardone, using the planetary model, showed qualitative agreement with Mendenhall's conclusions. Cardone's results also suggested that baroclinicity was more significant than stability in determining the veering of the wind in the planetary boundary layer. For both cases in situations of strong, cold advection the actual wind may back with height, especially in conjunction with unstable stratification.

Additional results on the influence of baroclinicity came from a study by Clarke (1970), who found a tendency for the boundary layer wind to back instead of veer with height in unstable conditions. He stated that this could have been due to baroclinicity or to acceleration. He noted that it could have occurred if $\frac{\partial \tau_*}{\partial z}$ was systematically

negative in convective conditions up to a level of about 0.2 $\frac{U_*}{f}$ instead of being positive as in the normal case. This latter interpretation was based on the observation that the wind appeared to be subgeostrophic in the convective layer and reached geostrophic values only after a rapid increase through the overlying inversion.

III. COMPUTATIONS AND NUMERICAL PROCEDURES

A. EXTERNAL WIND FIELD SPECIFICATIONS

All computations were made with data defined on a subset of the FNWC 63X63 grid which covered the North Pacific Ocean (Figure 9). Data fields included sea level pressure, sea surface temperature, and surface air temperature at each of 315 grid points spaced 381 km apart at 60°N. The necessary map factor was included for a 1:30 million polar stereographic projection.

The coriolis term appears as an external parameter and therefore poses a limitation on the lowest geographical latitude where the geostrophic relation would be valid. It has already been established that the dynamic boundary layer was formed by the surface stress and the coriolis acceleration. Pushistov (1970) concluded that manifestations of the nonlinearity in the dynamics of the boundary layer and the appearance of a perceptible ageostrophic component of velocity in the free atmosphere were to be expected near latitudes of 7-10°. Sheppard (1970) suggested 20°N as a limiting latitude for application to boundary layer models. A limiting value of 15° latitude was used in this program as the limit on geostrophic flow. For latitudes below 15°, the coriolis parameter would be kept constant.

1. Geostrophic Wind Computations

The geostrophic wind components were computed from the surface pressure field (P) as follows

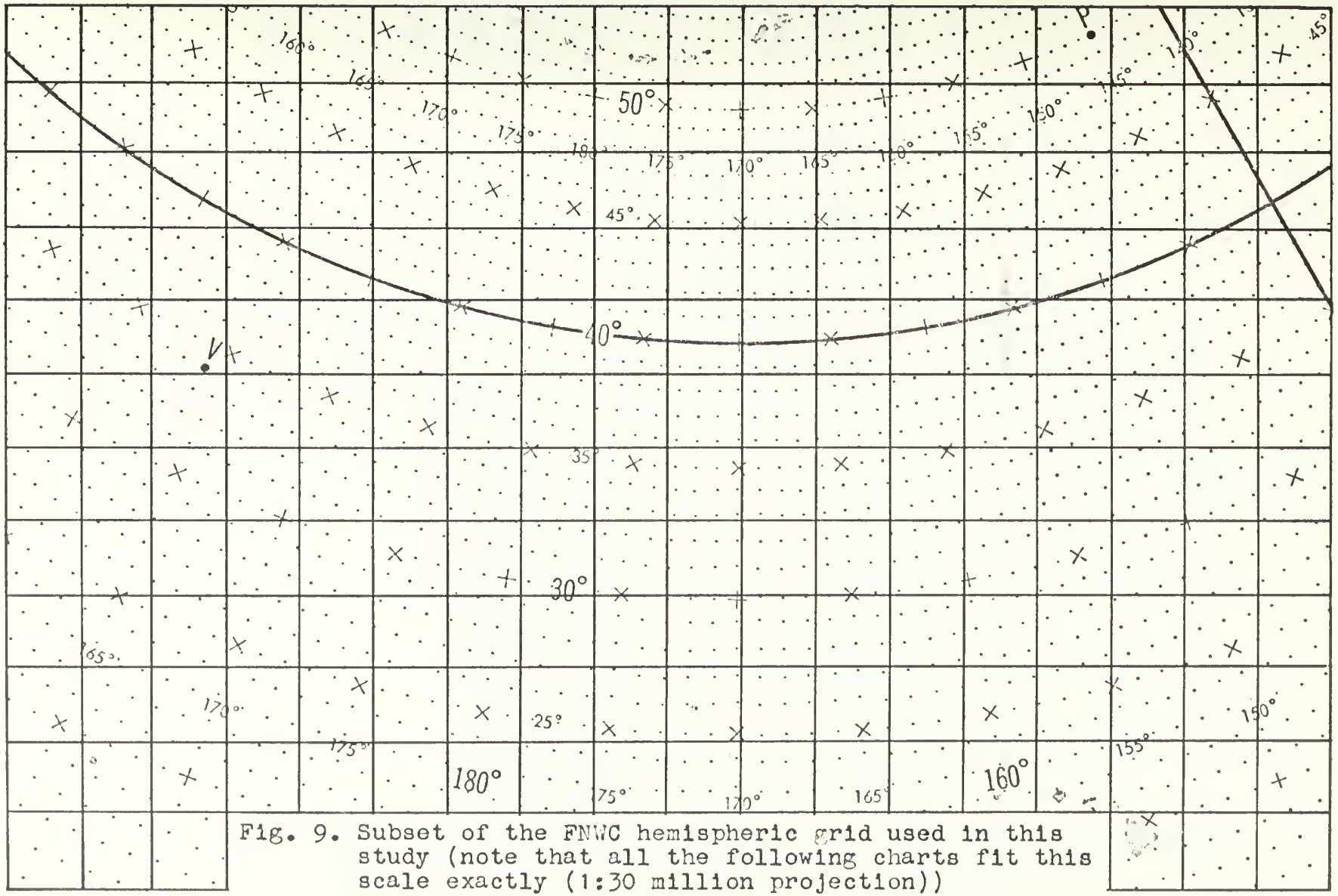

Fig. 9. Subset of the FNWC hemispheric grid used in this study (note that all the following charts fit this scale exactly (1:30 million projection))

$$u_g = - \frac{1}{\overline{\rho}_a f} \frac{\partial P}{\partial y} \tag{52}$$

$$v_g = \frac{1}{\overline{\rho}_a f} \frac{\partial P}{\partial x} \tag{53}$$

using a centered explicit finite difference technique. The density was determined from the equation of state

$$\overline{\rho}_a = \frac{P}{R_d \theta_a} \tag{54}$$

where R_d is the gas constant for dry air, and θ_a the surface air temperature in degrees Kelvin. The magnitude of the geostrophic wind was computed at each grid point from

$$|G| = \sqrt{u_g^2 + v_g^2} \quad . \tag{55}$$

2. Correction for Curvature

A gradient wind was calculated to correct for the effect of curvature on the surface geostrophic wind. Two basic principles were required for this correction. The first was that following an air parcel along an isobar, the total derivative was zero or

$$dP(x,y) = 0. \tag{56}$$

The second requirement was the mathematical statement of curvature

$$K_c(x,y) = \frac{y''}{[1 + (y')^2]^{3/2}} = \frac{1}{R} \tag{57}$$

where y' and y" were the first and second derivatives with respect to x, and R was the radius of curvature. By expanding the total derivative of

P, obtaining y' and y", and rearranging, the following result was obtained for the radius of curvature

$$R = \frac{\left(\frac{\partial P}{\partial y}\right)^2 \left[1 + \left(\frac{\partial P/\partial x}{\partial P/\partial y}\right)^2\right]^{3/2}}{\frac{\partial P}{\partial x}\left[2\frac{\partial^2 P}{\partial x\,\partial y} - \frac{\partial^2 P}{\partial y^2}\frac{\partial P/\partial x}{\partial P/\partial y}\right] - \frac{\partial P}{\partial y}\frac{\partial^2 P}{\partial x^2}} \quad . \tag{58}$$

Next the gradient wind was computed from

$$V_G = G - \frac{V_G^2}{fR} \quad . \tag{59}$$

Solving for V_G and rearranging led to a workable form of the equation

$$V_G = \frac{G}{1/2 + \sqrt{1/4 + G/Rf}} \quad . \tag{60}$$

For this case the magnitude of the term G/Rf determined how much curvature would be allowed. The maximum values were chosen to be -3/16 for anticyclonic curvature and +3/4 for cyclonic curvature which yielded a range of $V_G = 1.33G$ for anticyclonic curvature and $V_G = 0.67G$ for cyclonic curvature. This agreed with generally accepted synoptic limits.

Subroutine GRADWD (Appendix A) makes the necessary computations and follows a similar scheme utilized by FNWC (Kaitala, 1971 unpublished). Centered finite difference schemes were used to calculate the derivatives.

3. Thermal Wind Correction

The nondimensional thermal wind components were determined from

$$u_T = -\frac{g}{f^2\,\overline{\theta}_a}\frac{\partial \theta}{\partial y} \tag{61}$$

$$v_T = \frac{g}{f^2 \overline{\theta}_a} \frac{\partial \theta}{\partial x} , \qquad (62)$$

and the total thermal wind was given by

$$r = \sqrt{u_T^2 + v_T^2} . \qquad (63)$$

For this model, r had a limiting value of 100. The geostrophic and thermal wind angles were calculated from the previously computed wind components. This procedure was repeated for each grid point and was used as input data to the boundary layer model.

B. PROCEDURES IN SOLVING THE BOUNDARY LAYER EQUATIONS

1. Initial Conditions

a. Geostrophic Wind Speed Less Than Or Equal to 5.0 meters/second:

This case was associated with the aerodynamically smooth flow region described earlier. For this case no corrections were made for stability and a constant drag coefficient of 0.022 was assumed. This resulted in a constant inflow angle of 15°. The 19.5 meter wind was determined from

$$U_{19.5} = 0.7G \qquad (64)$$

The choice of the drag coefficient was not arbitrary, but depended on the relationship between C_z and U_z (see Figure 2). The value of C_{10} was a minimum at 6 meters/second under neutral conditions. The value of $C_{19.5}$ was extrapolated from this curve.

b. Geostrophic Wind Speed Greater Than 5.0 meters/second and Absolute Value of Air-Sea Temperature Difference Less Than or Equal to 1°C:

Initially the drag coefficient was $C_z = 0.0245$, with the thermal wind (r) and the angle between the geostrophic and thermal wind (η) set equal to zero. For this case L_*, L' and $\Psi(h/L')$ were set equal to zero and $\phi_u(h/L') = 1.0$. A solution was then obtained using the modified baroclinic model of Blackadar described below.

c. Geostrophic Wind Speed Greater Than 5.0 meters/second and Absolute Value of Air-Sea Temperature Difference Greater than 1° C:

The drag coefficient $C_z = 0.0245$ is used to estimate the initial U_* and r and η are set equal to zero. $\theta_a - \theta_s$ was restricted to the range -15 to +4.0°C. The values of L_*, L', $\Psi(h/L')$, and $\phi_u(h/L')$ were computed from z_a, $\theta_a - \theta_s$ and U_* and a solution was obtained using the modified Blackadar model described below.

L_* was computed from (34) and L' from (15) using as a first approximation

$$\Psi(z_a/L') = 10 - \ln(z_a/z_o) . \qquad (65)$$

$\Psi(h/L')$ was computed from SUBROUTINE PSI (Appendix A). If L_* was greater than zero (stable case), then

$$\Psi(h/L') = 0.7\, L_* \qquad (66)$$

If L_* was less than or equal to zero (unstable case), a value of Richardson number and $\phi_u(h/L')$ had to be computed. This was accomplished in SUBROUTINE SHR (Appendix A). Then $\Psi(h/L')$ was calculated from (13).

$\phi_u(h/L')$ was computed using SUBROUTINE SHR (Panofsky, 1968; Cardone, 1969). If L_* was greater than zero (stable case), then

$$\phi_u(h/L') = 1 + 7L_* \tag{67}$$

If L_* was less than or equal to zero (unstable case), then a new Richardson number was determined from

$$Ri_{new} = L_* (1 - 18 Ri_{old})^{1/4} \tag{68}$$

where initially $Ri_{old} = L_*$. This iteration was continued until the inequality

$$\left| Ri_{new} - Ri_{old} \right| < \epsilon \tag{69}$$

was satisfied, where $\epsilon = 0.01$ for this model. Then $\phi_u(h/L')$ was found from

$$\phi_u(h/L') = \frac{1}{(1 - 18 Ri_{new})^{1/4}} . \tag{70}$$

2. The Modified Blackadar Baroclinic Boundary Layer Model

The basis of this model was an iteration procedure which included the effects of stability and baroclinicity on the computed wind. The procedure was free of computational instability and converged rapidly for all reasonable choices of initial U_*. First values of z_o,

p, p', s, q, α, γ, Ψ_o, and $U_{*_{new}}$ were obtained using respectively equations (23), (35), (38), (43), (44), (45), (46), (50), and (51). The iterative procedure was repeated until the inequality

$$\left| U_{*_{new}} - U_* \right| \leq \epsilon \tag{71}$$

was satisfied where ϵ was 0.05. The iteration was repeated, setting $U_* = U_{*_{new}}$, until the inequality was again satisfied. If L_* was not zero, then new values of Ψ, z_o, and L'_{new} were computed where the argument of Ψ was z_a/L'. If

$$\left| L'_{new} - L' \right| \geq 5 \tag{72}$$

then L' was set equal to L'_{new}. The model was repeated from where L_* was first calculated until the inequality was satisfied. After completing the iterations for the case where the thermal wind (r) and η were equal to zero, the computed values of r and η were substituted and the model was again repeated until all criteria were satisfied. If $L' \neq 0$, then $\phi(z/L')$ was computed as $\phi(19.5/L')$; otherwise $\phi(19.5/L')$ was set equal to zero. Finally the wind at 19.5 meters was determined from

$$U_{19.5} = \frac{U_*}{k} \left[\ln \frac{19.5}{z_o} - \Psi \left(\frac{19.5}{L'} \right) \right] \tag{73}$$

Values of $\theta_a - \theta_s$, G, z_o, z/L', Ψ_o, U_*, $U_{19.5}$, $\log R_o$, U_*/G, $U_{19.5}/G$ and R_i were then available for each grid point.

C. COMPUTATION OF INDEX OF REFRACTION CONSTANT

In this section possible relationships are considered between the refractive index structure constant and quantities dependent only on the wind speed and air-sea temperature difference. Specifically those quantities that can be predicted from the model considered in this study are examined.

The propagation of light waves and radio waves is affected primarily by air-density inhomogeneities and therefore by temperature fluctuations. One effect of these fluctuations is scintillation or rapid changes in intensity at a point. These are distortions caused by variations in the speed of propagation through turbulent elements having different densities, and hence different indexes of refraction. The refractive index structure constant (C_n^2) is the primary parameter characterizing the turbulent fluctuations of the atmospheric refractive index for scales from a few millimeters to several meters. If the quantity C_n^2 is known, calculations can be made on scintillation, beam spreading, and beam wander, all of which are important in describing light wave propagation.

A relation necessary in the formulation is the one-dimensional spectrum for temperature fluctuations in the inertial subrange described by Corrsin (1951)

$$\phi_\theta (K) = B \varepsilon^{-1/3} N K^{-5/3} \qquad (75)$$

where ε is the rate of dissipation of turbulent kinetic energy, N is a measure of the "smearing" of temperature inhomogeneities, B is an

empirical constant (= 0.81, Boston, 1970), and K is the streamwise component of wave number. The structure constant for temperature fluctuations (C_T^2) is defined as

$$C_T^2 = B\ \varepsilon^{-1/3}\ N \tag{76}$$

and is related to the index of refraction as follows

$$C_n^2 = \left(\frac{-79 \times 10^{-6}\ P}{T_a^2}\right)^2\ C_T^2\ . \tag{77}$$

Another expression which has to be considered is the nondimensional balance equation for turbulent kinetic energy, which, for stationary, horizontally homogeneous flow is (Busch and Panofsky, 1968)

$$\phi_u - {}^z/_L - \phi_\varepsilon - \phi_D = 0. \tag{78}$$

ϕ_u is the nondimensional wind shear (8), ϕ_D represents the divergence terms, and

$$\phi_\varepsilon = \frac{\varepsilon\, k z}{U_*^3}\ . \tag{79}$$

The following relations arise from the definitions in the nondimensional turbulent kinetic energy balance and definition of N

$$\varepsilon = \phi_\varepsilon\ \frac{U_*^3}{k z} \tag{80}$$

$$N = -\overline{\theta w}\ \frac{\partial \theta}{\partial z} = K_H\ \left(\frac{\partial \bar{\theta}}{\partial z}\right)^2\ . \tag{81}$$

Substitution of these two expressions, plus the definition of K_m (29) into the definition of C_T^2 yields (Panofsky, 1968)

$$C_T^2 = B\, \phi_\varepsilon^{-1/3}\ \left(\frac{K_H}{K_m}\right)\ \frac{1}{\phi_u}\ (k z)^{4/3}\ \left(\frac{\partial \bar{\theta}}{\partial z}\right)^2\ . \tag{82}$$

Equation (82) is not a suitable expression because of the lack of information on ϕ_ε . However if the effect of the divergence terms is neglected, ϕ_ε can be expressed in terms of ϕ_u and z/L as

$$\phi_\varepsilon = \phi_u - z/L . \tag{83}$$

It is noted that with wind-wave interaction, the assumption that the divergence terms can be neglected is probably not valid, but the possible effect this assumption has on predictions of C_T^2 has not been studied.

Substitution of (83) into (82) yields

$$C_T^2 = B \left[\phi_u - z/L\right]^{-1/3} \left[\frac{K_H}{K_m} \frac{1}{\phi_u}\right] (kz)^{4/3} \left(\frac{\partial \bar{\theta}}{\partial z}\right)^2 . \tag{84}$$

This final equation for C_T^2 lends itself to the boundary layer model because all the parameters can be computed within the model. Thus, the model can be used to obtain a horizontal distribution of C_T^2 over water for various wind and stability conditions. The average stability $\partial\theta/\partial z$ is determined from (14).

The ratio of the exchange coefficients K_H/K_m is set equal to 1.0 in Cardone's formulation. However it has been shown that K_H and K_m are not usually identical except for small values of $\partial\theta/\partial z$ for which the turbulent motion is not significantly influenced by buoyancy forces. Businger et al. (1971) suggested the following form for the ratio of eddy diffusions

$$a_h = 1.35 \frac{(1 - 9\, z/L)^{1/2}}{(1 - 15\, z/L)^{1/4}} . \tag{85}$$

Here $a_h = 1.35$ for neutral conditions, which agrees closely with laboratory measurements (cf., Hinze, 1959). A value of 1.35 rather than 1.0 for a_h under neutral conditions arises because the von Kármán constant was equal to 0.35 instead of the usual 0.40 (Businger et al., 1971).

D. WAVE HEIGHT ANALYSIS

Wave analysis is another application for the boundary layer model. For this purpose, a simplified version of the FNWC sea-swell model (Hubert and Mendenhall, 1970) was utilized. The u and v components of the 19.5 meter wind determined from the boundary layer model were used as both current and history input in this analysis.

The FNWC sea-swell model computes a weighted wind from the wind components as follows:

$$u = 0.3\, u_{t-12} + 0.7\, u_t$$

$$v = 0.3\, v_{t-12} + 0.7 v_t \qquad (86)$$

where t-12 is the 12-hour old history wind speed and t is the current wind speed. These component values are saved as history for the next analysis run, and then the total wind (V) is computed. The wave heights (W_A) in feet are then computed from

$$W_A = 7 \left[\left(\frac{V}{10}\right)^2 - \left(\frac{V}{20}\right)^{3.3} \right] + 1.0 \qquad (87)$$

Although this is a very simple empirical method for determining wave heights, the basic method has been used by FNWC since the mid-1960's and this particular model has been used operationally since August 1970.

In addition, the FNWC model computed corrections for fetch and ice, and performed some smoothing of the resulting height field. It was assumed these corrections would be minimal for this application.

IV. SPECIFICATION OF EXTERNAL PARAMETERS

A primary objective of this study was to apply the two-level baroclinic boundary layer model to actual atmospheric conditions and compare the computed results with the observed results. The time period 00 GMT 28 November 69 through 00 GMT 02 December 69, with an analysis interval of every 12 hours, was chosen for this comparison for several reasons. First an intense low pressure system, which influenced most of the central North Pacific Ocean, developed during this period with the system reaching maximum intensity about 00 GMT 30 November 69. The system provided input data which allowed the model to predict boundary layer parameters under varying atmospheric conditions. Secondly considerable synoptic data had been gathered by the author during an earlier study on the extreme sea conditions (unpublished) associated with this storm. The latter gave a good basis for comparing computed values to observed data. Finally, this storm produced waves and swell which caused considerable damage to several islands of the Pacific as well as to the spar buoy FLIP. Therefore a wave generation model was applied using the predicted surface winds, and these predicted waves were compared to the observed wave conditions.

The 00 GMT 30 November 69 period was of the most interest due to its extreme conditions, extensive data coverage, and it was the probable period when the destructive waves were being generated. The various corrections described above were incorporated into the model for this

time period, and synoptic data were plotted and analyzed for surface pressure, air-sea temperature difference, surface wind speed and wave height.

Surface layer parameters were computed including various combinations of stability, curvature, and thermal wind to yield information on the relative importance of each parameter in the formulation. The following notation will be used in describing the results:

NN - non-neutral, correction for stability

N - neutral - no stability correction

NC - no curvature correction applied

C - curvature correction applied

NT - no thermal wind correction applied

T - thermal wind correction applied

It was recognized at the onset of the study that the specification of the external fields ($\Delta\theta$ and G) had to be reasonably accurate in order to evaluate the model on the basis of observed wind fields. For example, if the observed surface winds were quite different than those predicted by the model, some estimate had to be available on the possibility that the discrepancies were due to poor specification of the geostophic wind or the air-sea temperature difference. Therefore in this section consideration is given to the relevant aspects of representing those fields which make up the external parameters.

The charts in the following figures correspond to a 1:30 million polar stereographic projection with the grid as depicted in Figure 9.

A. FNWC ANALYSIS

Sea level pressure and air-sea temperature difference fields for 00 GMT 30 November appear in Figure 10. A 967 mb low pressure center was located near 45°N 180° with considerable thermal instability both ahead of and behind the system. A significant feature of this system was the intense isobaric gradient in the western quadrant.

The first consideration was the comparison of the computed surface geostrophic wind with the computed gradient wind for this period. The geostrophic and gradient wind fields computed from the surface pressure fields in Figure 10 appear in Figures 11 and 12 (units of meters/second). Figure 13 depicts the influence of the curvature correction on the geostrophic wind computed as a percent difference from geostrophic wind minus gradient wind then divided by geostrophic wind.

The two maximum wind centers west and north of the Low are based on data at one grid point and result from the influence of anticyclonic curvature, strong isobaric gradients, and finite difference computations. These features do not appear to be realistic. However, the wind speed distribution depicted by them is good except that the magnitude of the wind speed may be a little too large. It was expected that the maximum change would occur in an area of maximum curvature and maximum pressure gradient from the relation in (60). Generally speaking, the change in wind speed due to the curvature correction is 10 to 20% with a maximum change of 34% imposed by the limits placed on the term G/Rf in (60).

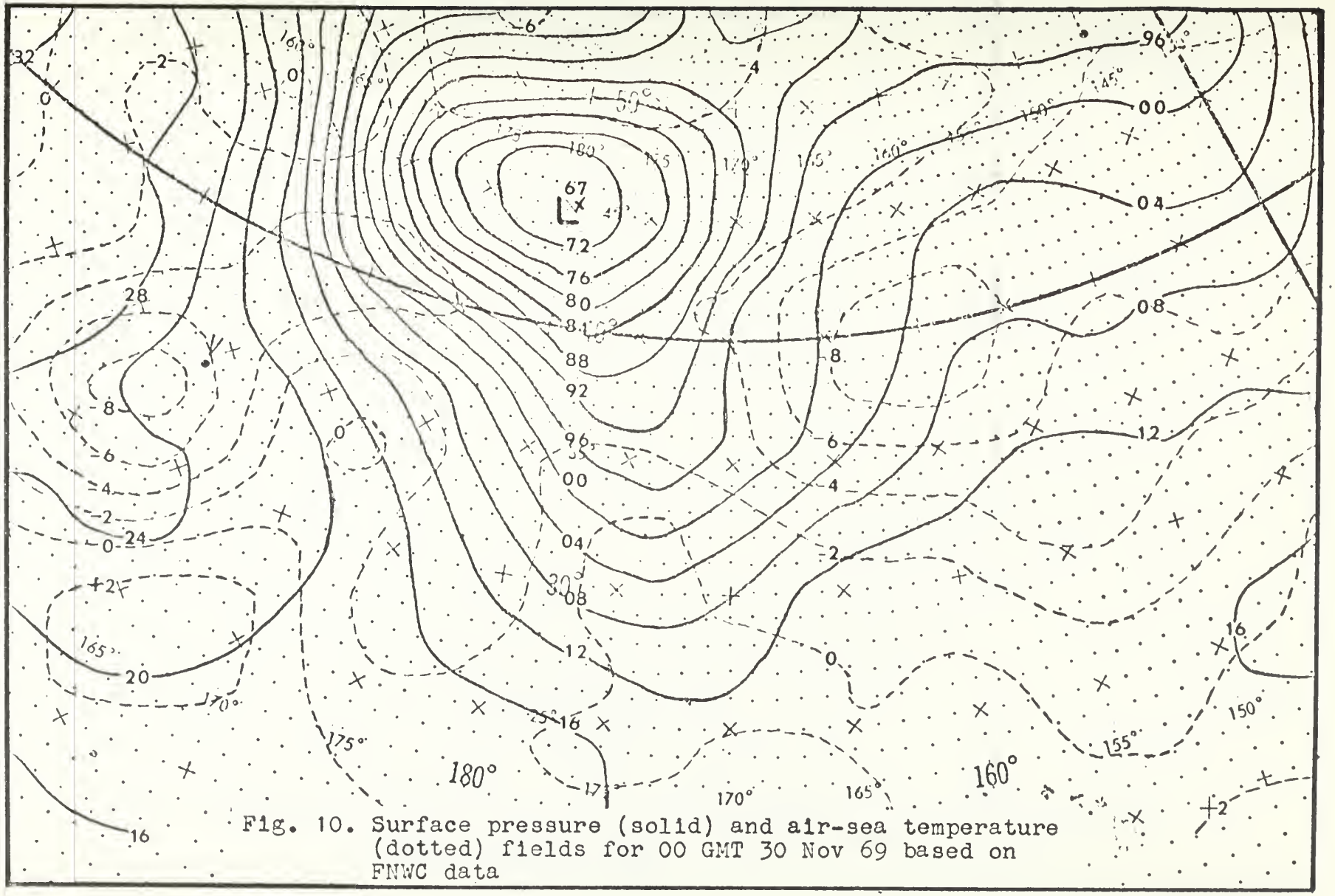

Fig. 10. Surface pressure (solid) and air-sea temperature (dotted) fields for 00 GMT 30 Nov 69 based on FNWC data

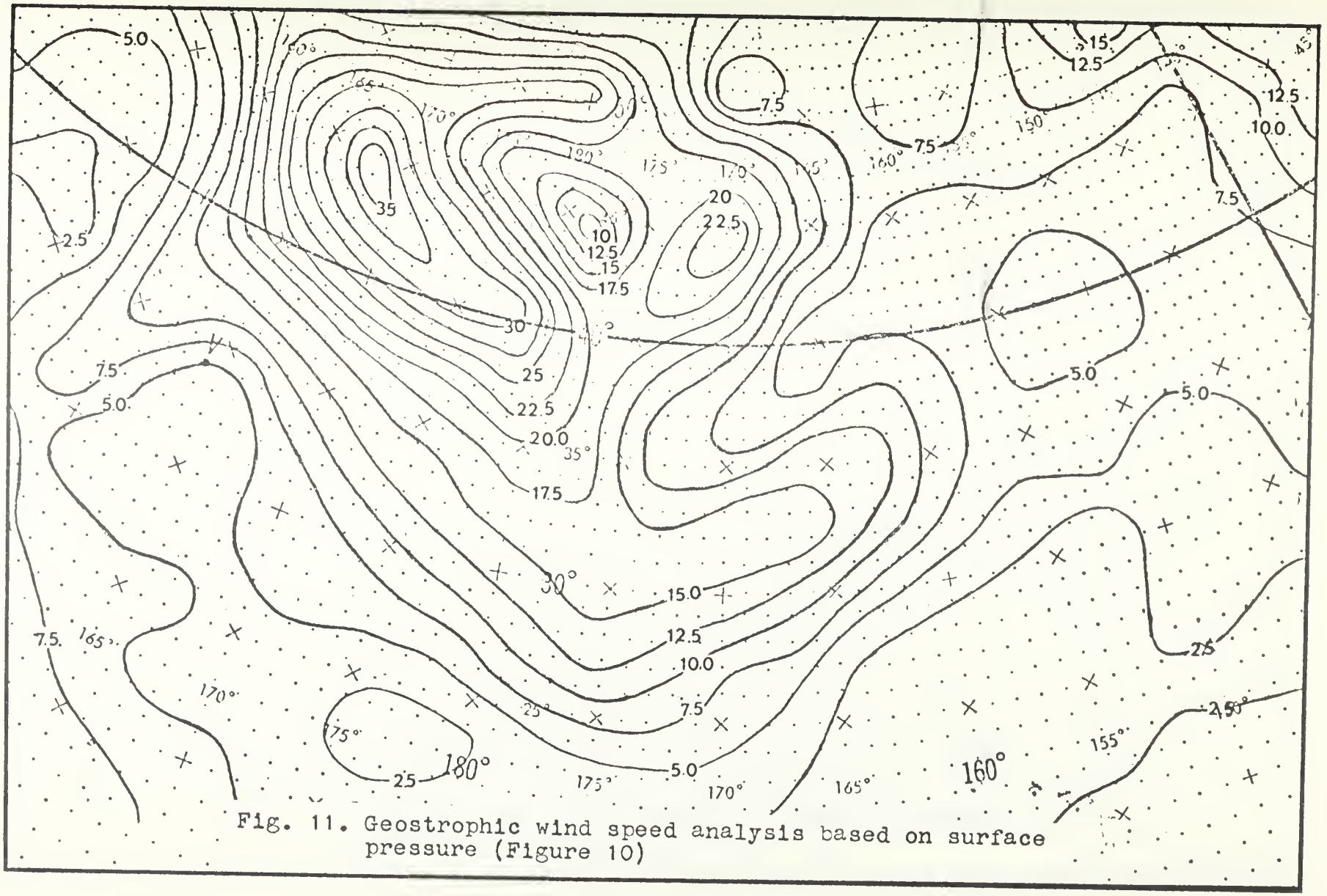

Fig. 11. Geostrophic wind speed analysis based on surface pressure (Figure 10)

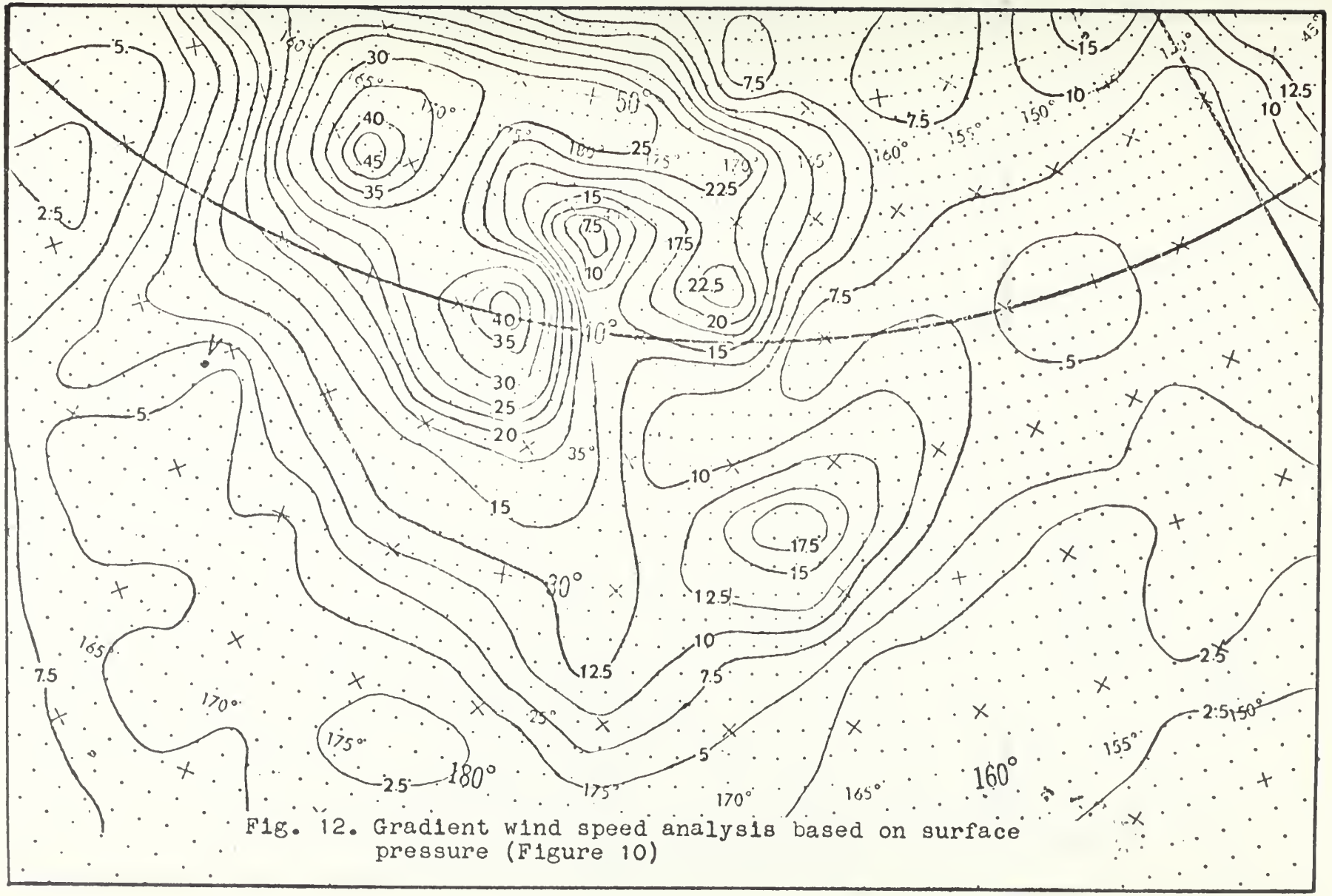

Fig. 12. Gradient wind speed analysis based on surface pressure (Figure 10)

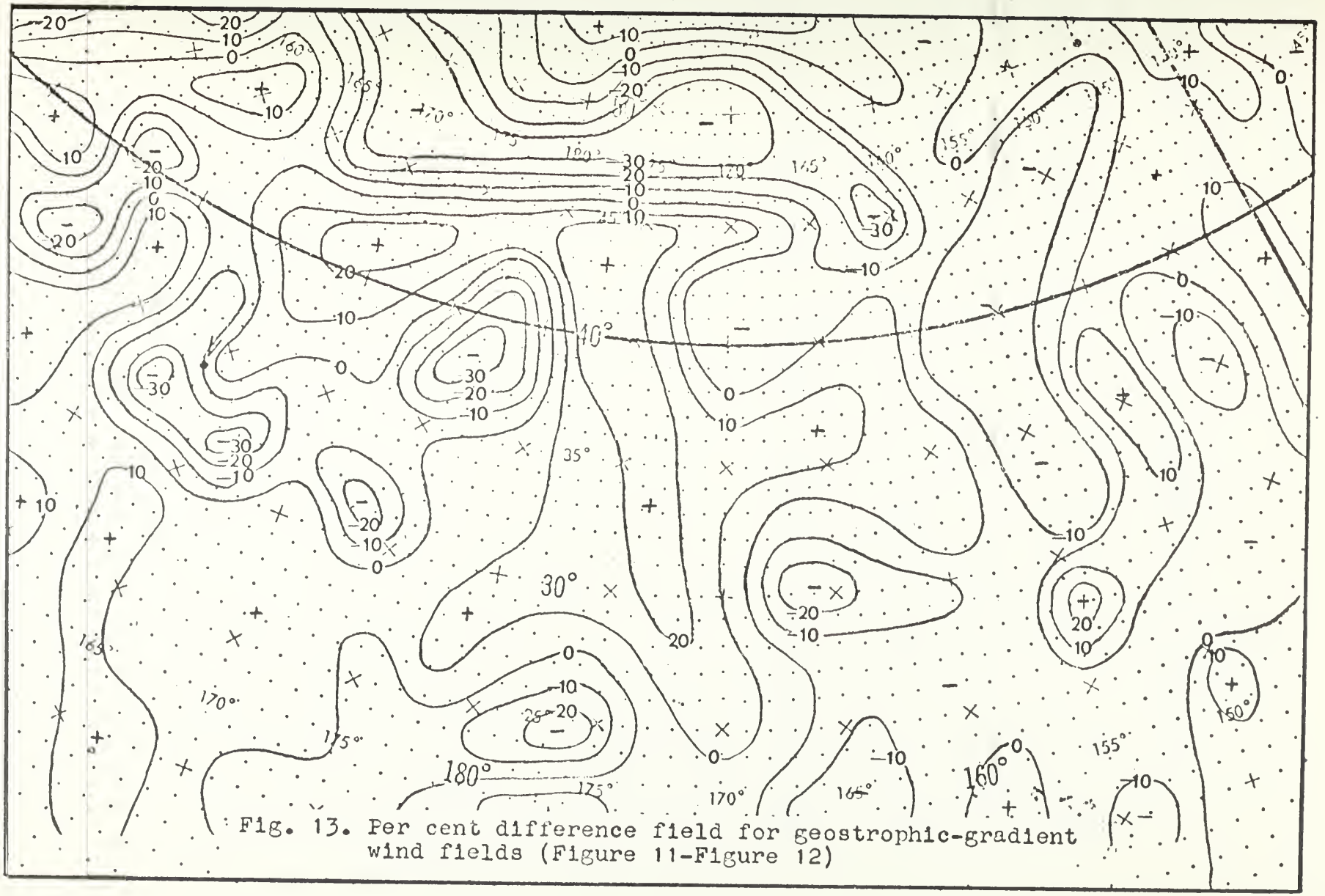

Fig. 13. Per cent difference field for geostrophic-gradient wind fields (Figure 11-Figure 12)

B. SUBJECTIVE ANALYSIS

The results from the hand analyzed surface chart were also used in comparisons of results. Figure 14 illustrates the surface pressure and air-sea temperature difference fields from the subjective analysis which are analogous to Figure 10. The major variations between Figure 10 and 14 appear to be due to the difference in the number of synoptic reports used as well as the analysis scheme. Theoretically, Figure 14 should be more representative since more data were included, but it was a subjective analysis. Figures 15 and 16 depict the geostrophic and gradient surface winds computed from the subjectively analyzed pressure field.

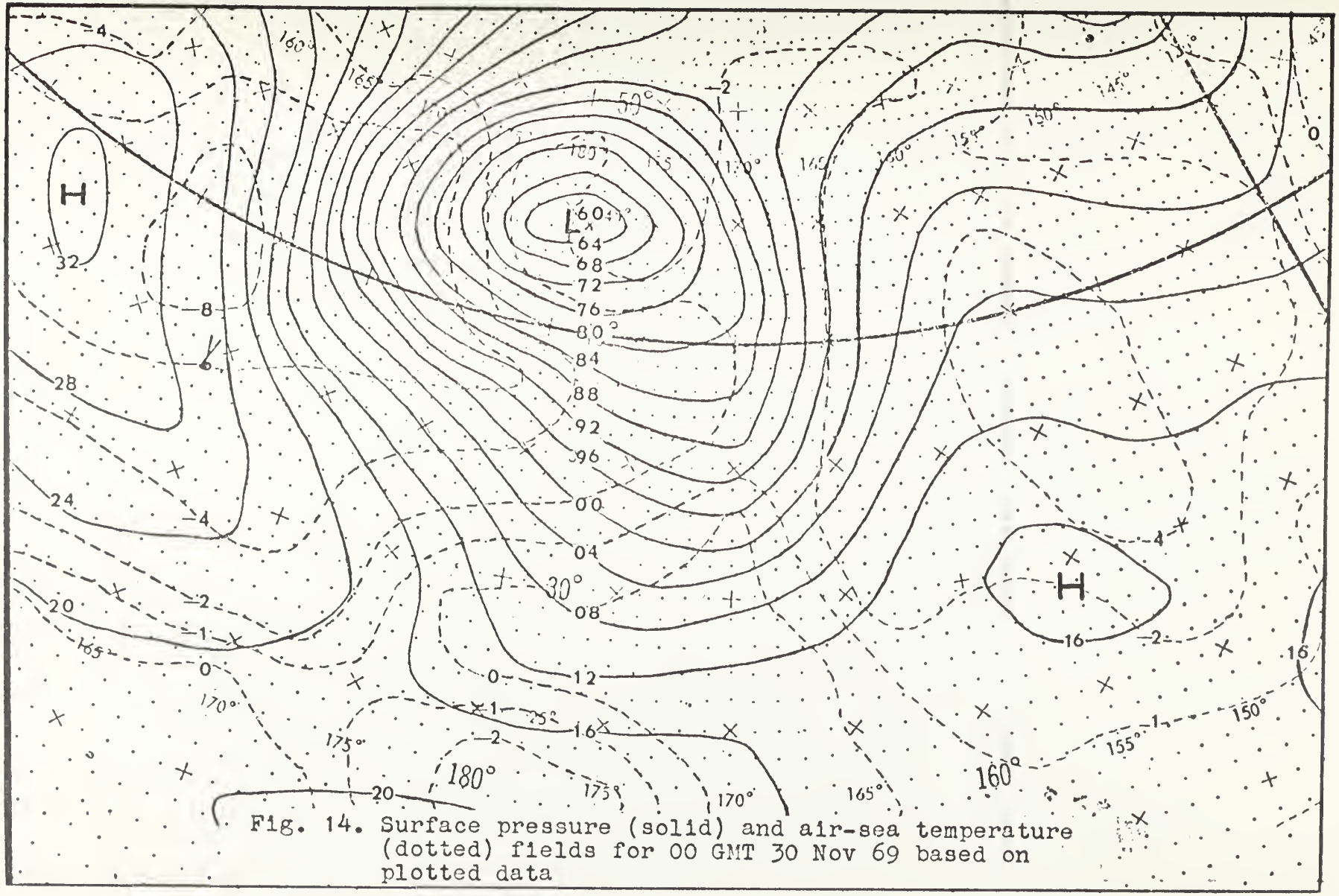

Fig. 14. Surface pressure (solid) and air-sea temperature (dotted) fields for 00 GMT 30 Nov 69 based on plotted data

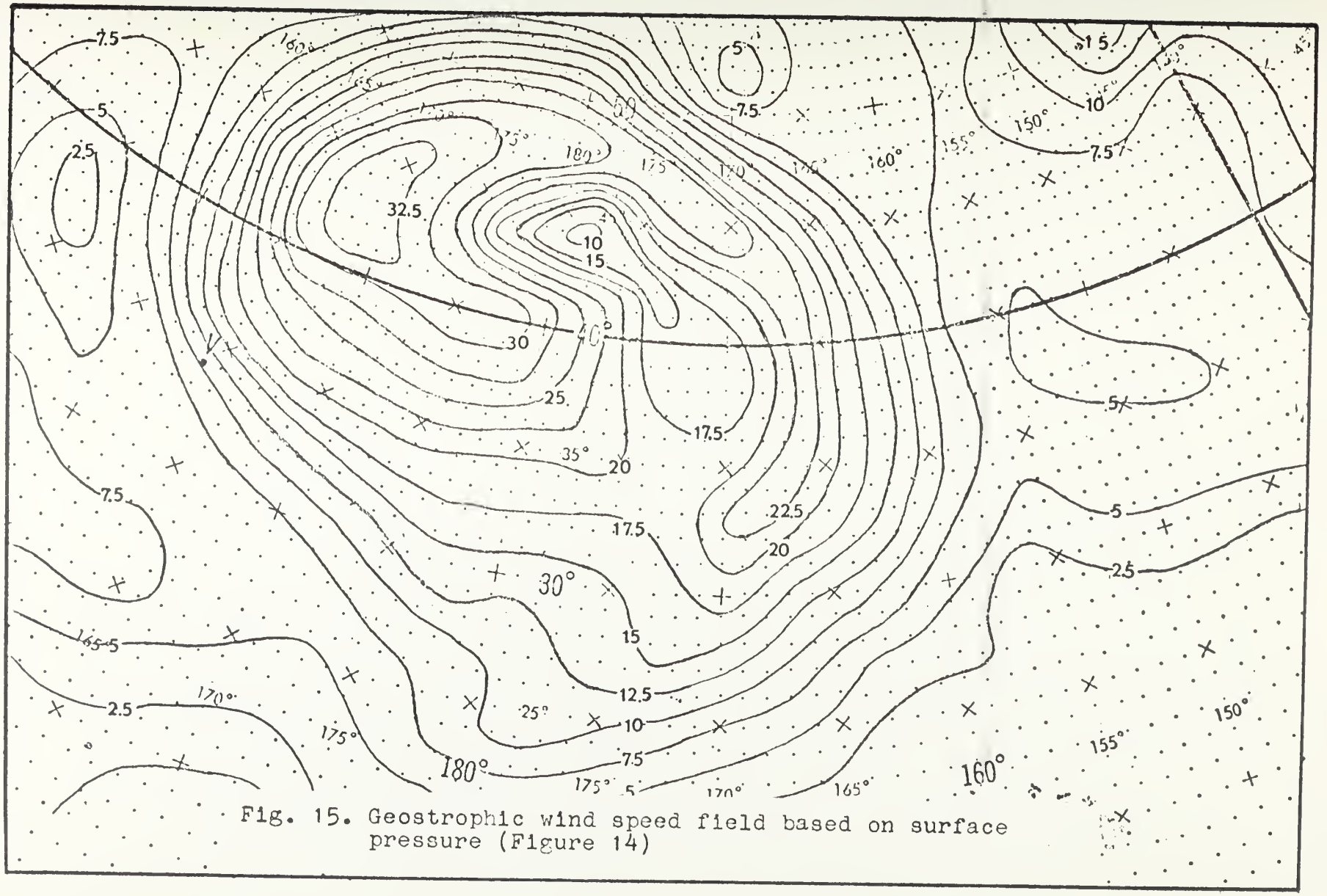

Fig. 15. Geostrophic wind speed field based on surface pressure (Figure 14)

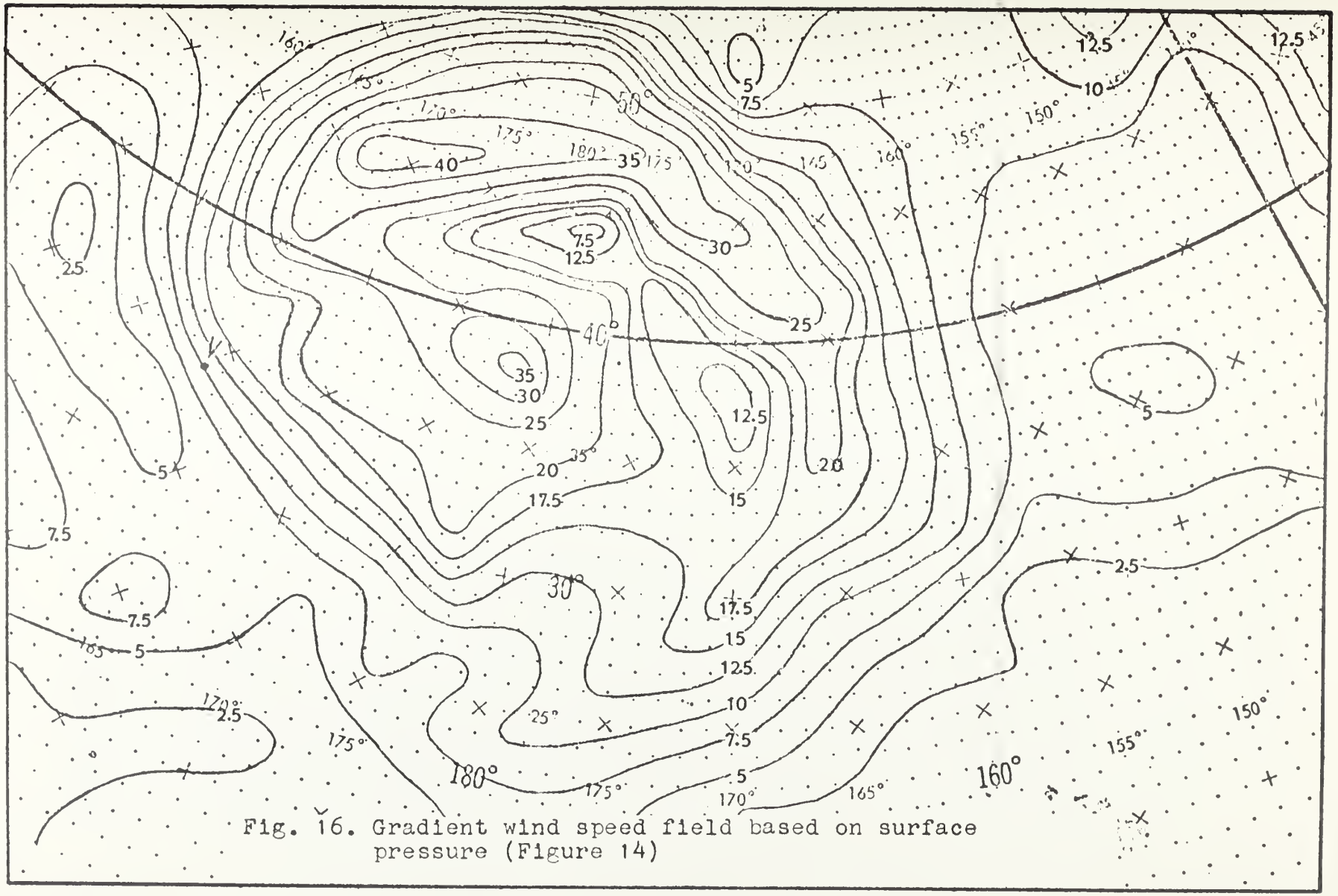

Fig. 16. Gradient wind speed field based on surface pressure (Figure 14)

V. RESULTS FROM EXPERIMENTS WITH THE MODEL

A. COMPARISONS IN TERMS OF SURFACE ROSSBY NUMBER AND STABILITY CATEGORIES

Near surface parameters were computed for the 19.5 meter level. This level represents an average height of ship anemometers (Bunting, 1968). Theoretically the computed 19.5 meter level winds could be compared with the observed wind fields and this would yield some information on the accuracy of the model in predicting surface winds.

In order to verify the computations and also to examine the range of conditions provided by the data, a comparison was made with Cardone's results which appear in Figures 4 and 5. Results for this comparison were obtained from computations in which stability was included but not baroclinicity. Results from all nine time periods appear in Figures 17 and 18 where values of the logarithm of the surface Rossby number (24) range from 7.76 to 9.45. The U_*/G versus log R_o results (Figure 17) agree with Cardone's results (Figure 4) except with regards to the interval between L_* isolines. In Figure 17 this interval (spacing) is larger. With respect to Ψ_o versus log R_o (Figure 18), the unstable results (negative L_*) agree with those in Figure 5 except, again, with regards to the interval between L_* isolines. The stable results (positive L_*), however, deviate considerably from Cardone's results with the veering angle decreasing as L_* increases. The results in Figure 18 would

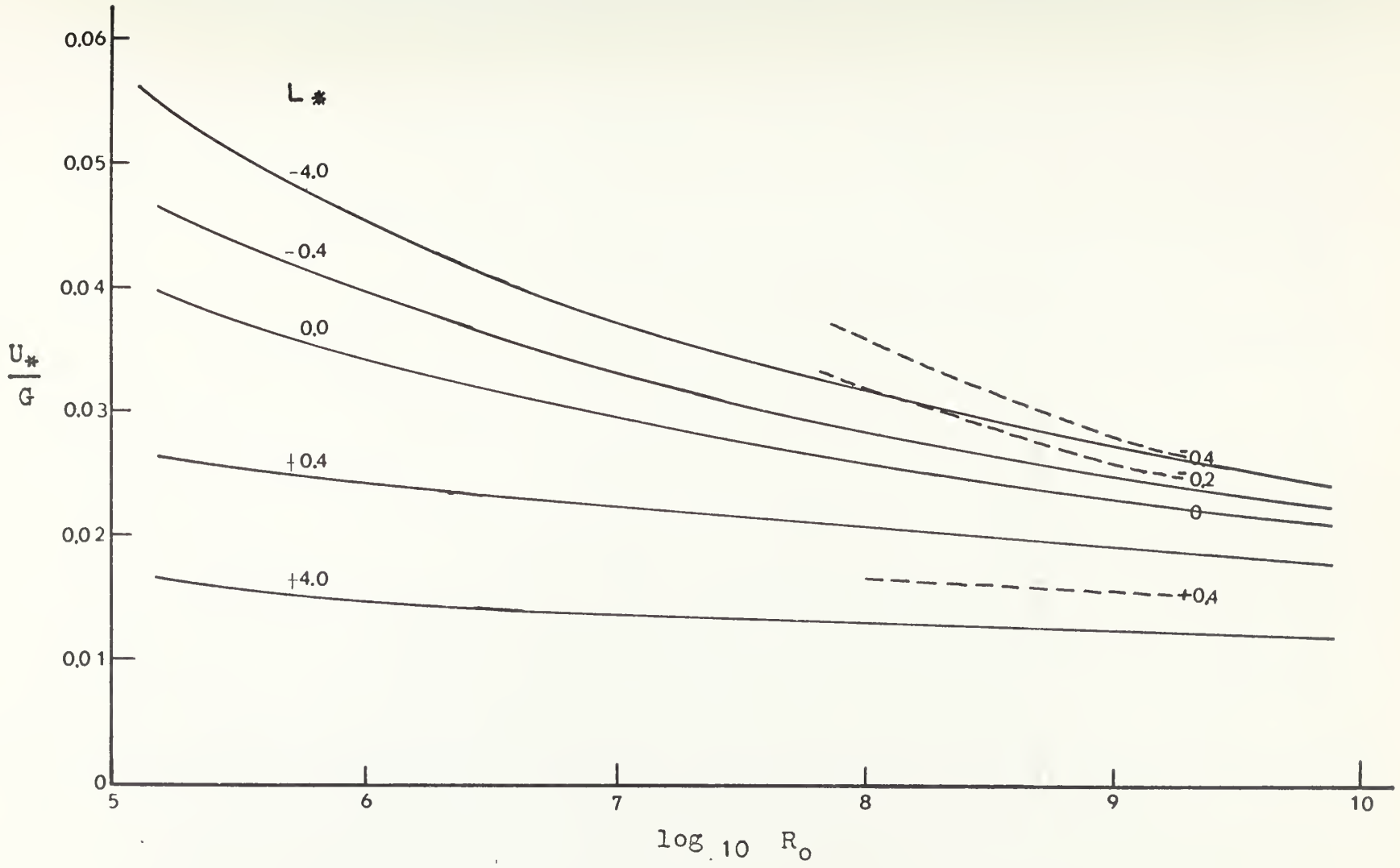

Fig. 17. Same as Figure 4 except dotted lines are results from this study

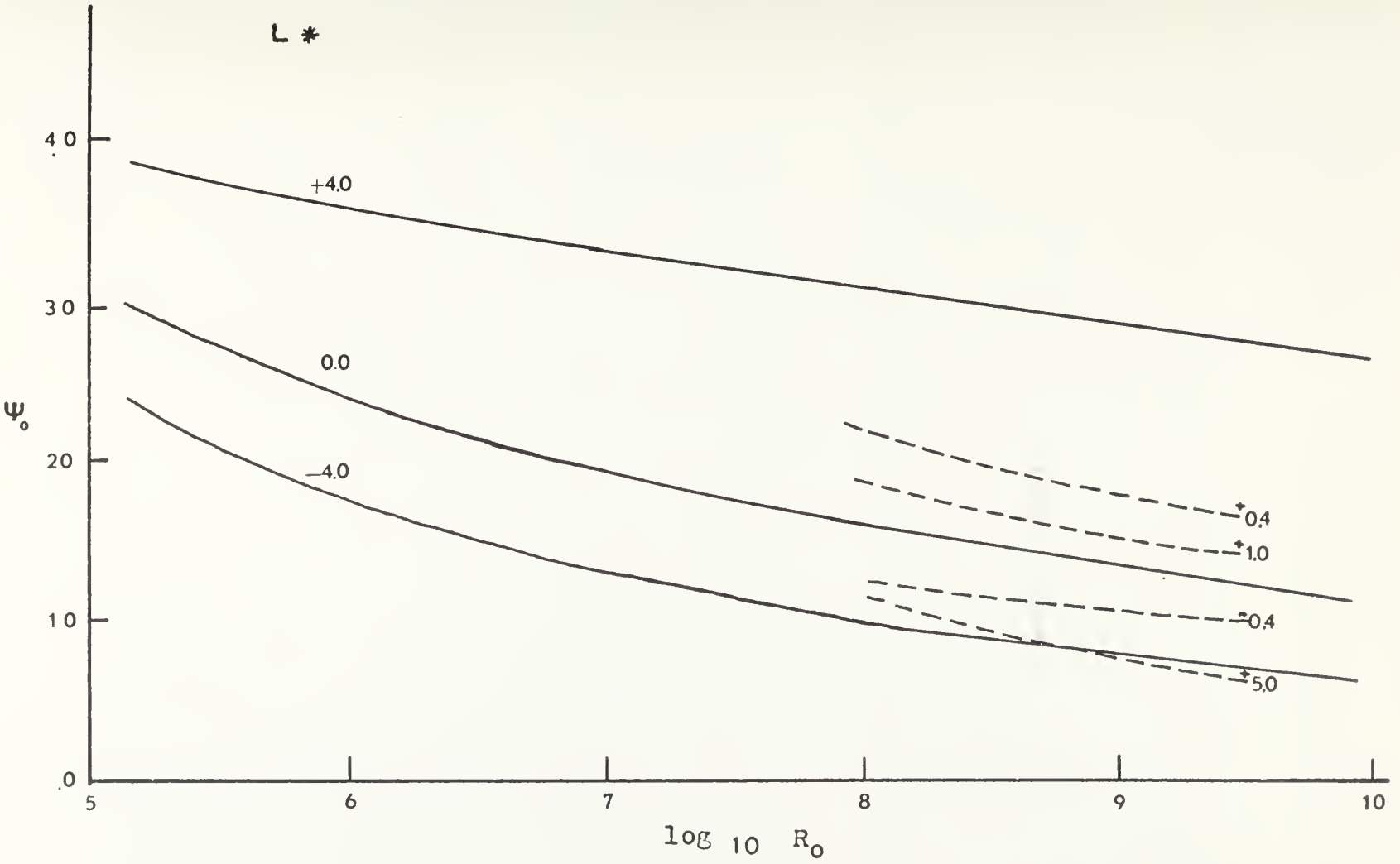

Fig. 18. Same as Figure 5 except dotted lines are results from this study

indicate that the veering angle decreases with both increasing stability and increasing instability with a discontinuity occurring near neutral conditions.

The unusual, and unexpected, features in the results just described were examined in considerable detail. The same results were noted by Pafias (unpublished study, 1971) in an investigation with Cardone's program. These features in the results are perhaps related to the drag coefficient representation selected by Cardone and also because different iteration limits were used in this study than those used by Cardone.

The range of data with respect to U_*/G and $\theta_a - \theta_s$ was also examined and the results appear in Figure 19. The computations for these results were made on the basis of a barotropic atmosphere with no correction for isobaric curvature. These computations differ from those used by Cardone for Figure 8 in that a variable coriolis parameter was used. Isolines have been drawn for geostrophic wind speeds ranging from 15 to 75 knots. For those wind speeds considered by Cardone in Figure 19, and also for wind speeds above 20 knots considered by Pafias, these results are in agreement. The change in shape of the curves for winds under 20 knots was not described by Cardone but is probably due to a combination of the functional forms for the stability dependence and the drag coefficient as chosen by him.

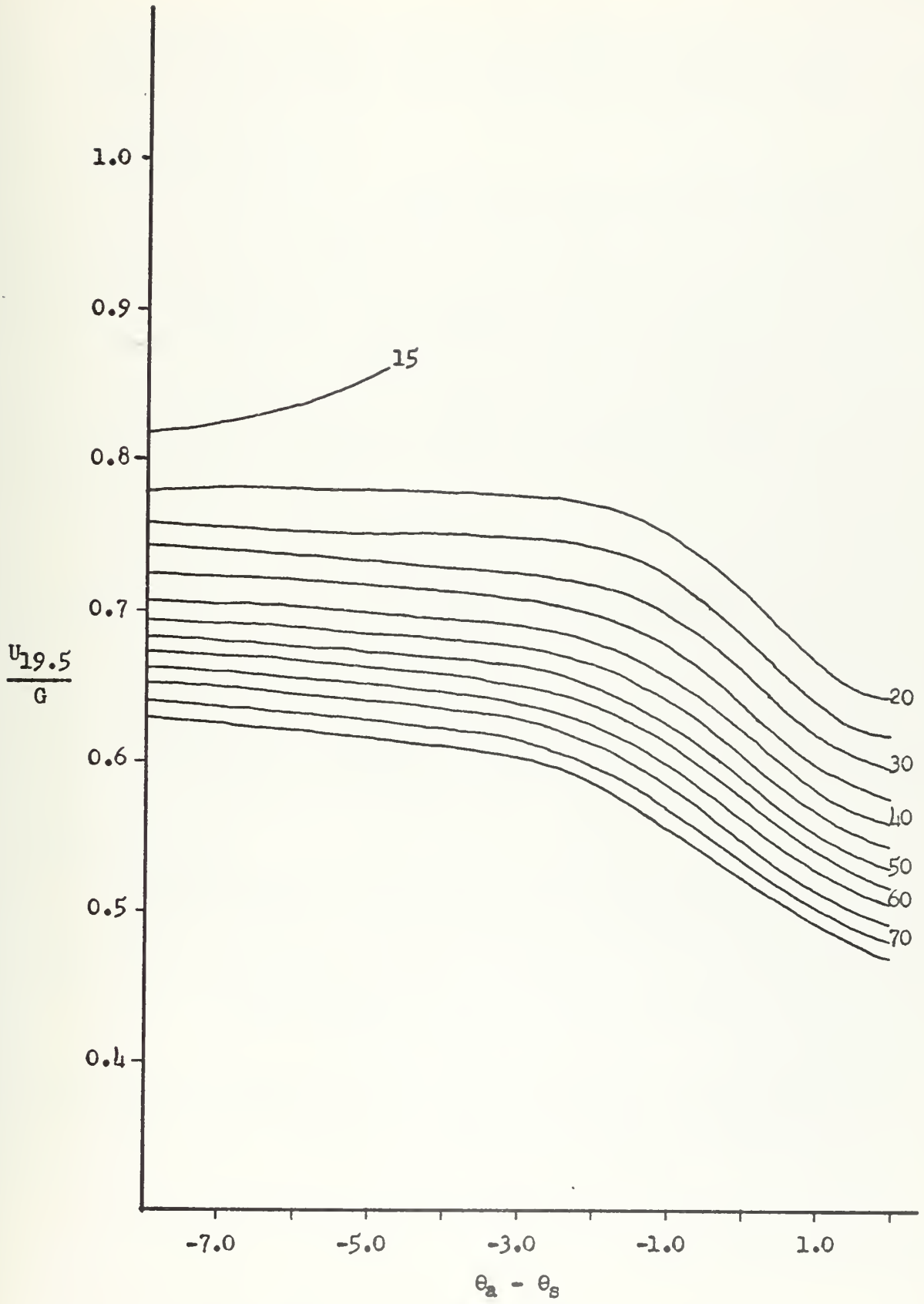

Fig. 19. Geostrophic drag coefficient versus air-sea temperature difference for range of geostrophic wind

B. EXPERIMENTS WITH CHANGING THE PHYSICS IN THE TWO-LAYER MODEL AND CHANGING THE SPECIFICATION OF THE SURFACE GEOSTROPHIC WIND

In this section $U_{19.5}$ results which were obtained from different computations with the two-layer model are compared. These computations were varied by including or not including specific parameters or corrections. The variations considered and compared were described earlier and are 1) N/NC/NT, 2) NN/NC/NT, 3) NN/NC/T, 4) NN/C/T, and 5) NN/NC/T with $k = 0.35$.

These variations will be referred to as Cases 1 through 5. It is noted that if the geostrophic wind speed was less than or equal to 5.0 meters/second, stability and baroclinicity were not taken into account in the iteration schemes. In regions with this wind speed range, especially in the subtropics, differences will not arise except where isobaric curvature exists.

Per cent difference (1-2) will be used to compare the two cases where (1-2) corresponds to the following computation at each grid point:

$$\frac{\text{case 1 result - case 2 result}}{\text{case 1 result}} \times 100 \ .$$

Although large differences between cases were unexpected, small corrections at low wind speeds could produce large per cent changes.

The surface wind fields corresponding to each of the five cases are presented in the following paragraphs along with selected comparisons between pairs of cases.

Case 1 (N/NC/NT)

This is the simplest case with respect to the possible physics which are included in the model. The external wind field is defined for a neutral, barotropic atmosphere with no curvature correction. The wind field at 19.5 meters for this case appears in Figure 20.

Case 2 (NN/NC/NT)

The effects of stability are now included and the 19.5 meter wind field for this case appears in Figure 21. The per cent difference (2-1) field is shown in Figure 22. Positive values correspond to increases in the computed $U_{19.5}$ field due to including the stability effect. This increase is quite evident on the western side of the cyclone. The patterns are not expected to be coincident with the air-water temperature isolines in Figure 10 because the stability effect is dependent on both the temperature gradient and the wind speed. The 20% contours near the eastern border are attributed to small corrections at low wind speeds as discussed previously.

Case 3 (NN/NC/T)

The effects of including the baroclinicity or thermal wind are now included and the 19.5 meter wind field for this case appears in Figure 23. The per cent difference (2-3) field is seen in Figure 24. Negative values correspond to an increase in the computed 19.5 meter wind due to including the thermal wind in the model. In this difference field, only 20 grid points (6%) appeared to be significantly affected by including the thermal wind. These grid points generally lie in an area of warm air advection.

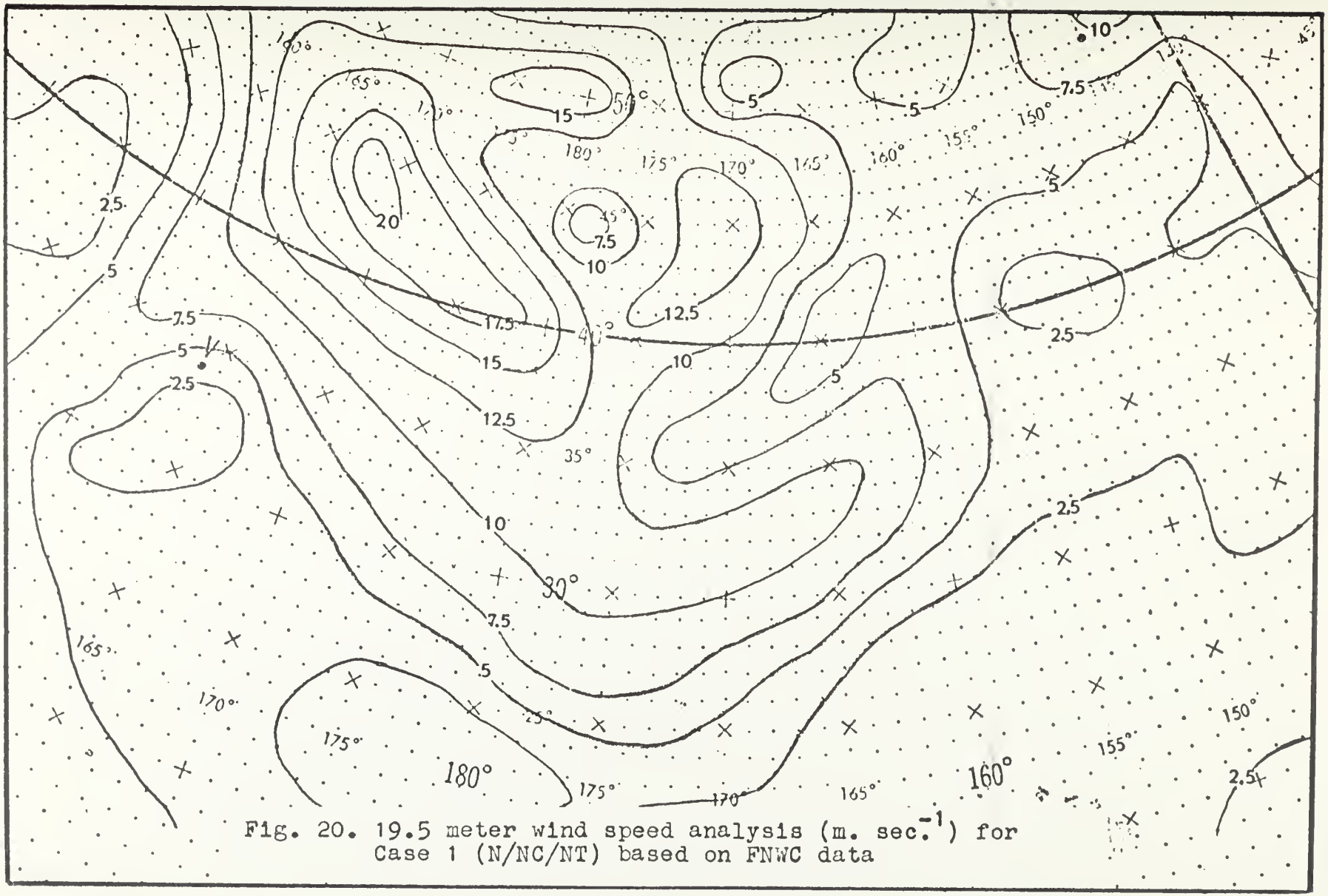

Fig. 20. 19.5 meter wind speed analysis (m. sec.$^{-1}$) for Case 1 (N/NC/NT) based on FNWC data

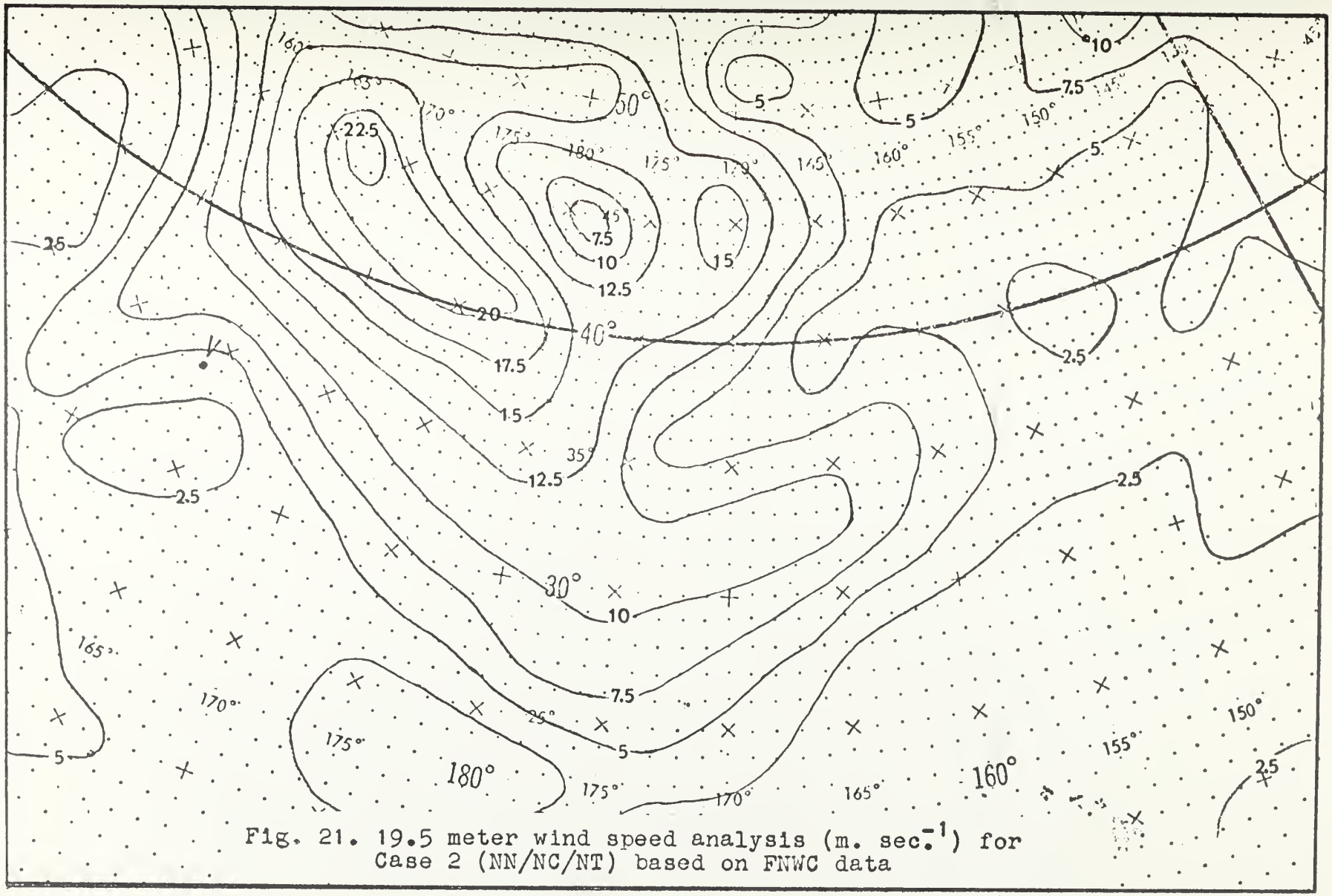

Fig. 21. 19.5 meter wind speed analysis (m. sec.$^{-1}$) for Case 2 (NN/NC/NT) based on FNWC data

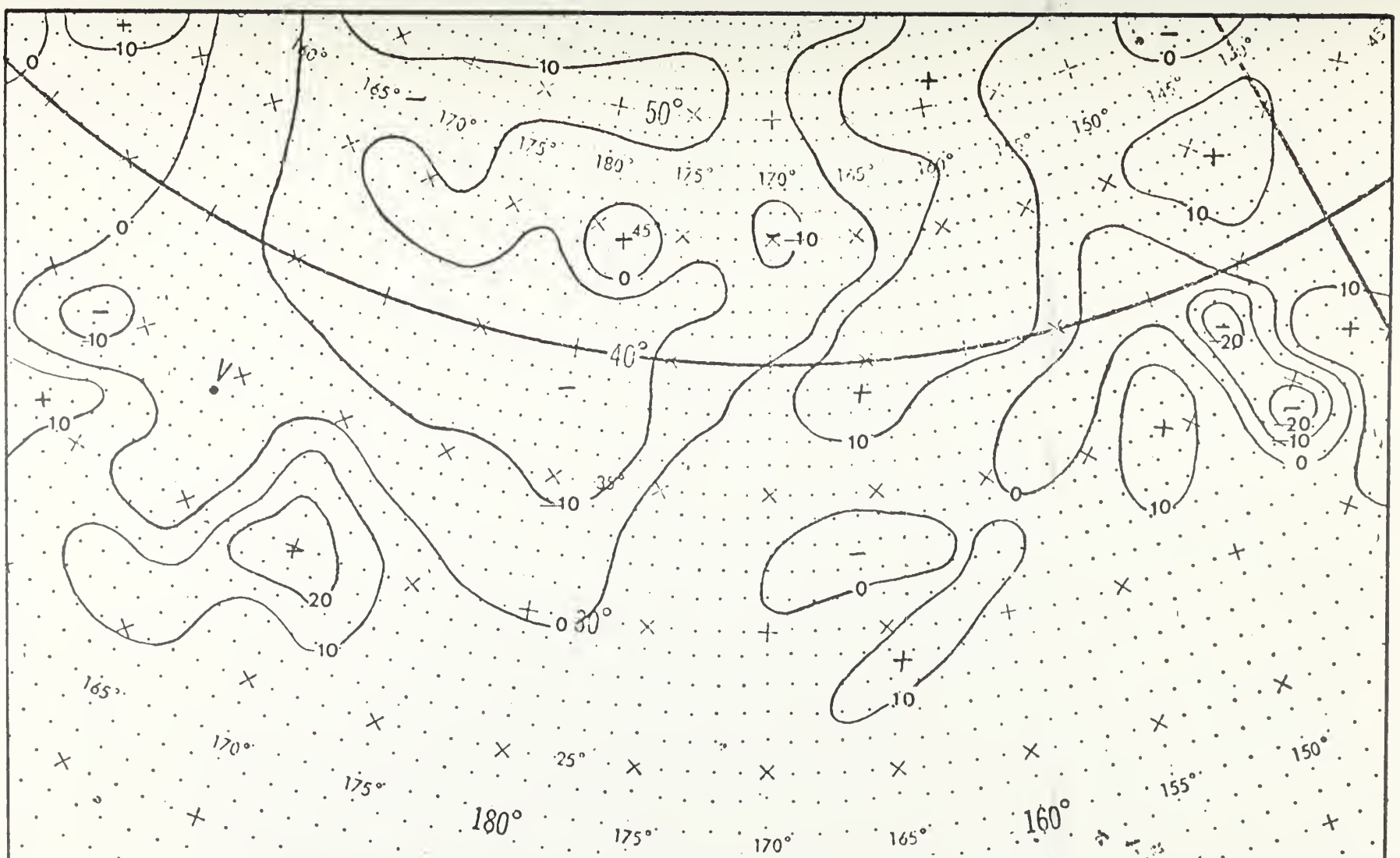

Fig. 22. 19.5 meter wind difference field (%) for Case 2 - Case 1. Positive % indicate increased wind speed due to stability

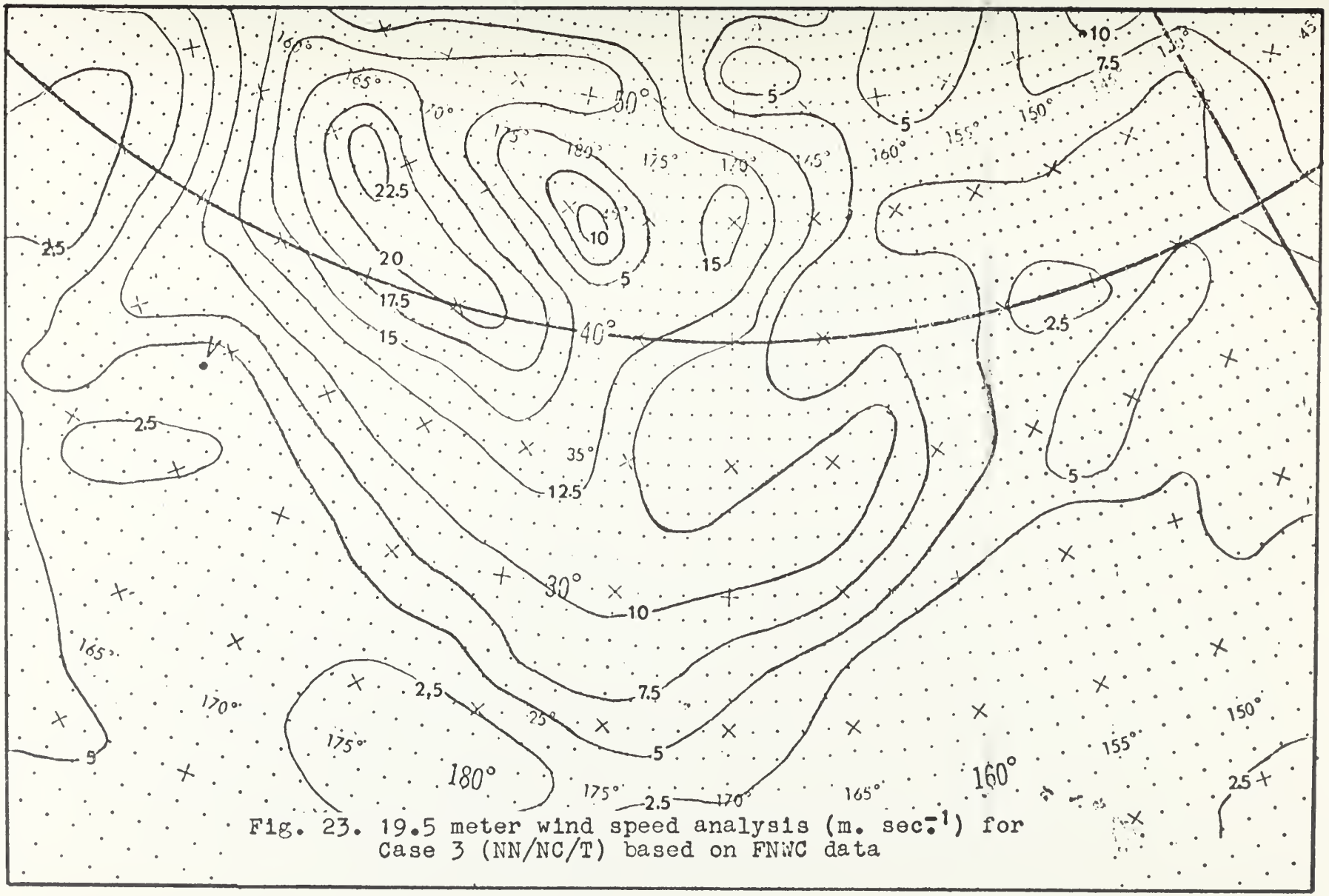

Fig. 23. 19.5 meter wind speed analysis (m. sec^{-1}) for Case 3 (NN/NC/T) based on FNWC data

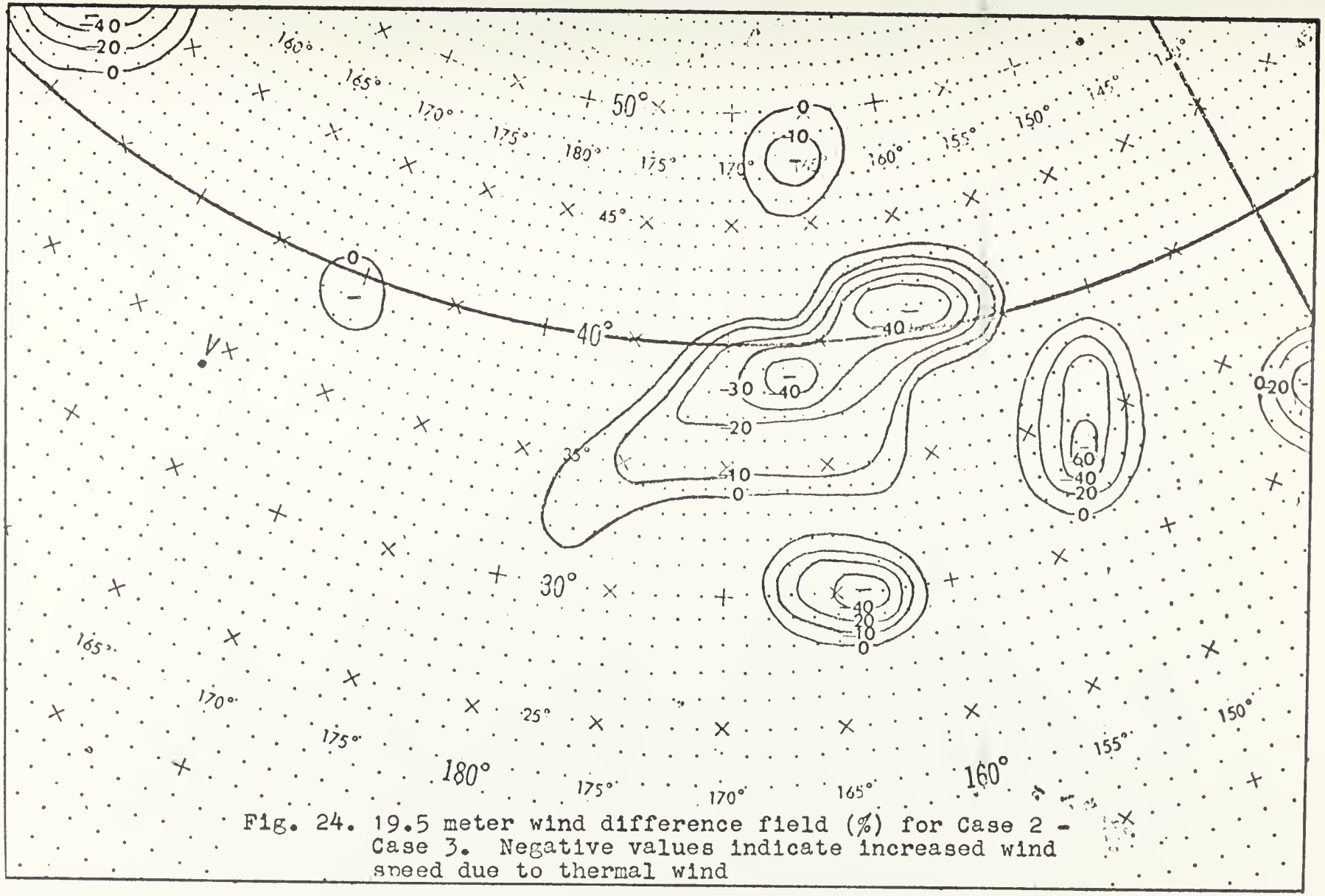

Fig. 24. 19.5 meter wind difference field (%) for Case 2 - Case 3. Negative values indicate increased wind speed due to thermal wind

Case 4 (NN/C/T)

In addition to all specifications possible within the physics of the model, the correction for curvature is applied to the external wind field. The 19.5 meter wind analysis for this field is shown in Figure 25 and the per cent difference field (3-4) appears in Figure 26. Negative values correspond to larger 19.5 meter winds due to including the curvature correction. Strong wind maximums, noted in comparing the external wind fields with and without this correction, also appear in Figure 26 as the predominant feature. In general, the effective change in the 19.5 meter wind field specification is larger and covers more area than any of the other cases.

Case 5 (NN/NC/T with k = 0.35)

This case differs from case 3 only with respect to the change of the von Kármán constant from 0.40 to 0.35. The 19.5 meter wind field for this case appears in Figure 27 and the per cent difference field (3-5) is depicted in Figure 28. Negative values correspond to increased 19.5 meter winds due to the change in the value of k. The suggested value of k = 0.35 arose from recent surface layer observational investigations by Businger et al. (1971). They noted from their results that using k = 0.40 in several empirical expressions led to estimates of U_* values which were 15% too high when compared with direct measurements of the momentum transfer. The fields in Figure 28 indicate that a general increase of 12 to 17% occurs in the computed 19.5 meter wind field if the lower value of k is used. This increase agrees with the U_*

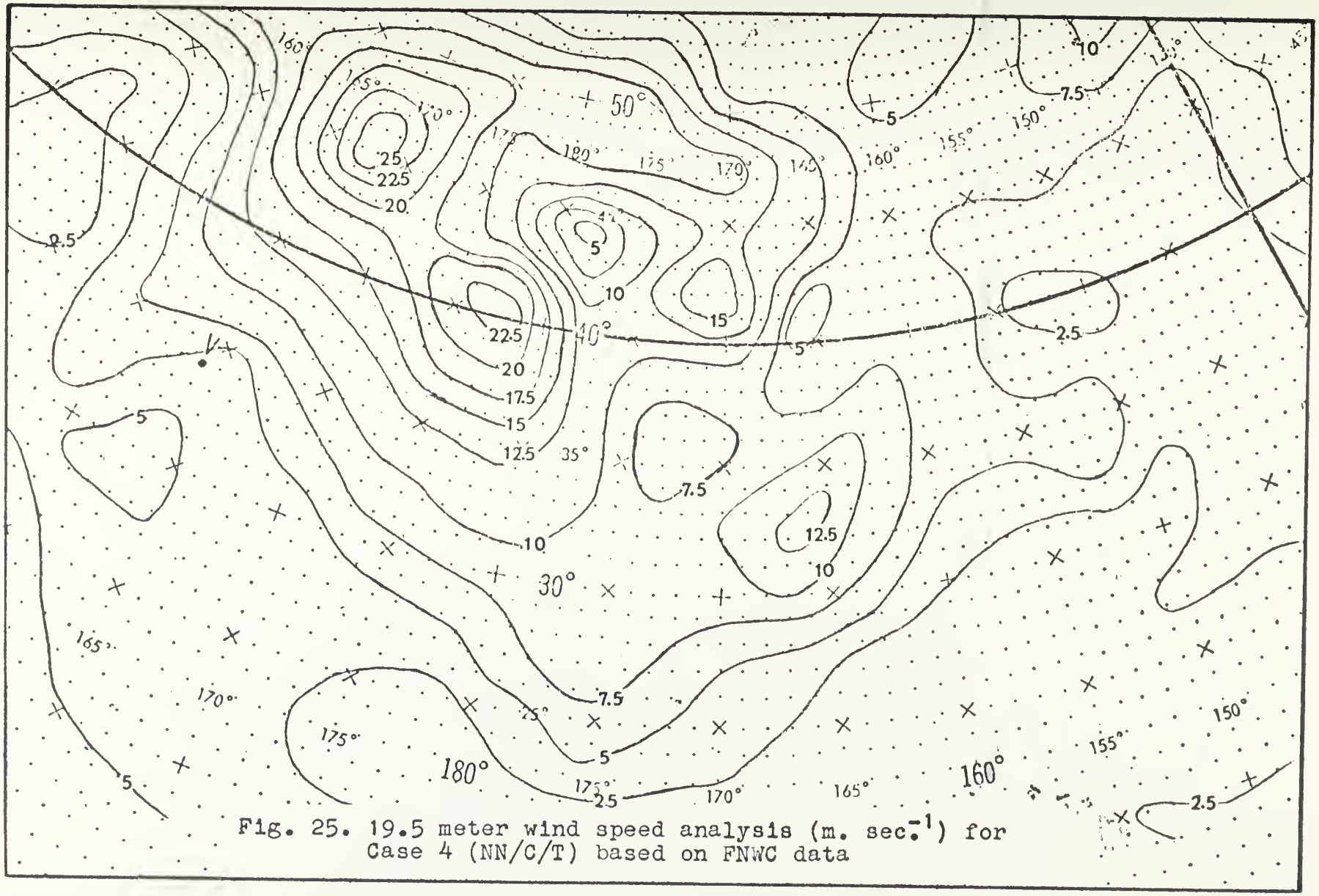

Fig. 25. 19.5 meter wind speed analysis (m. sec.$^{-1}$) for Case 4 (NN/C/T) based on FNWC data

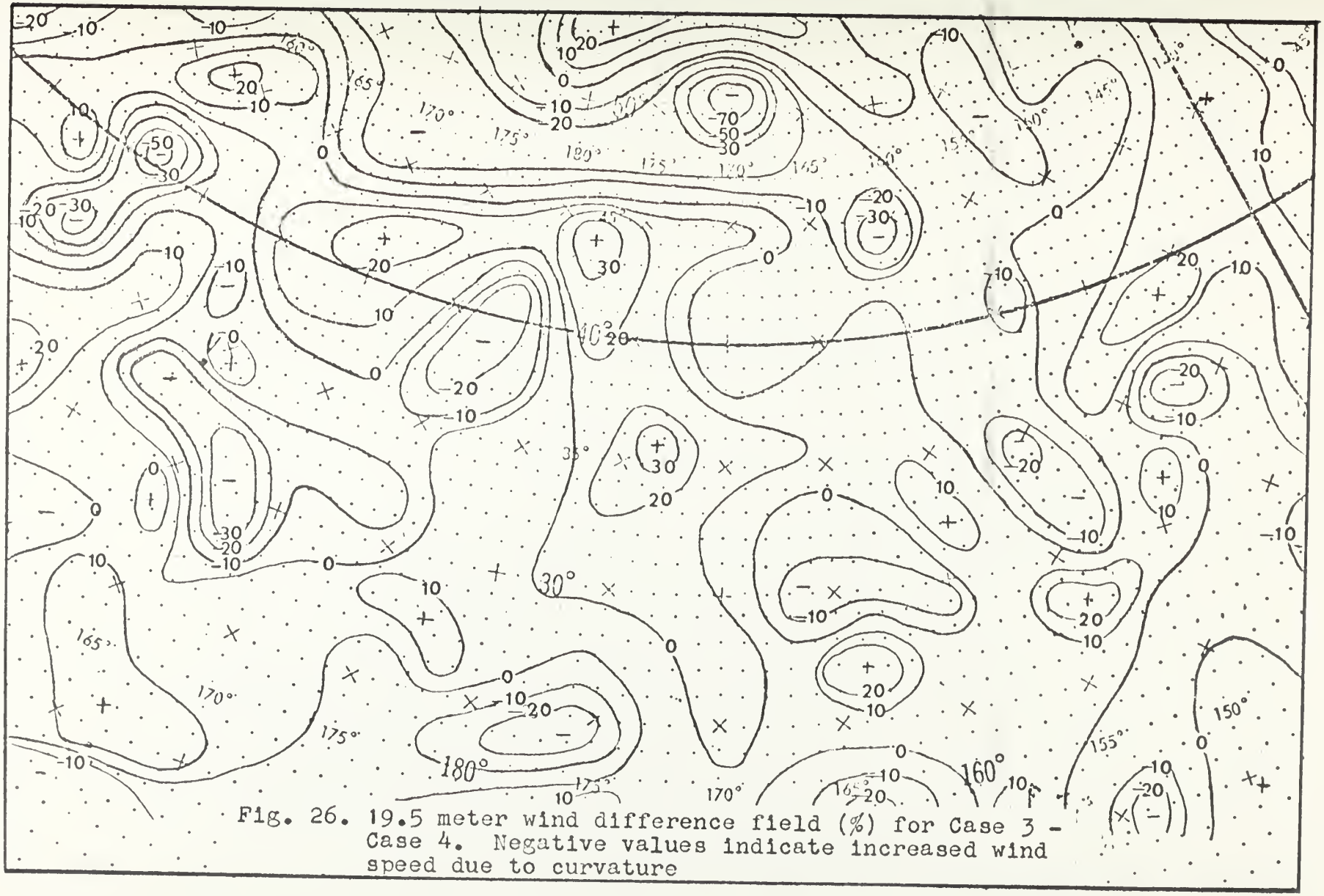

Fig. 26. 19.5 meter wind difference field (%) for Case 3 - Case 4. Negative values indicate increased wind speed due to curvature

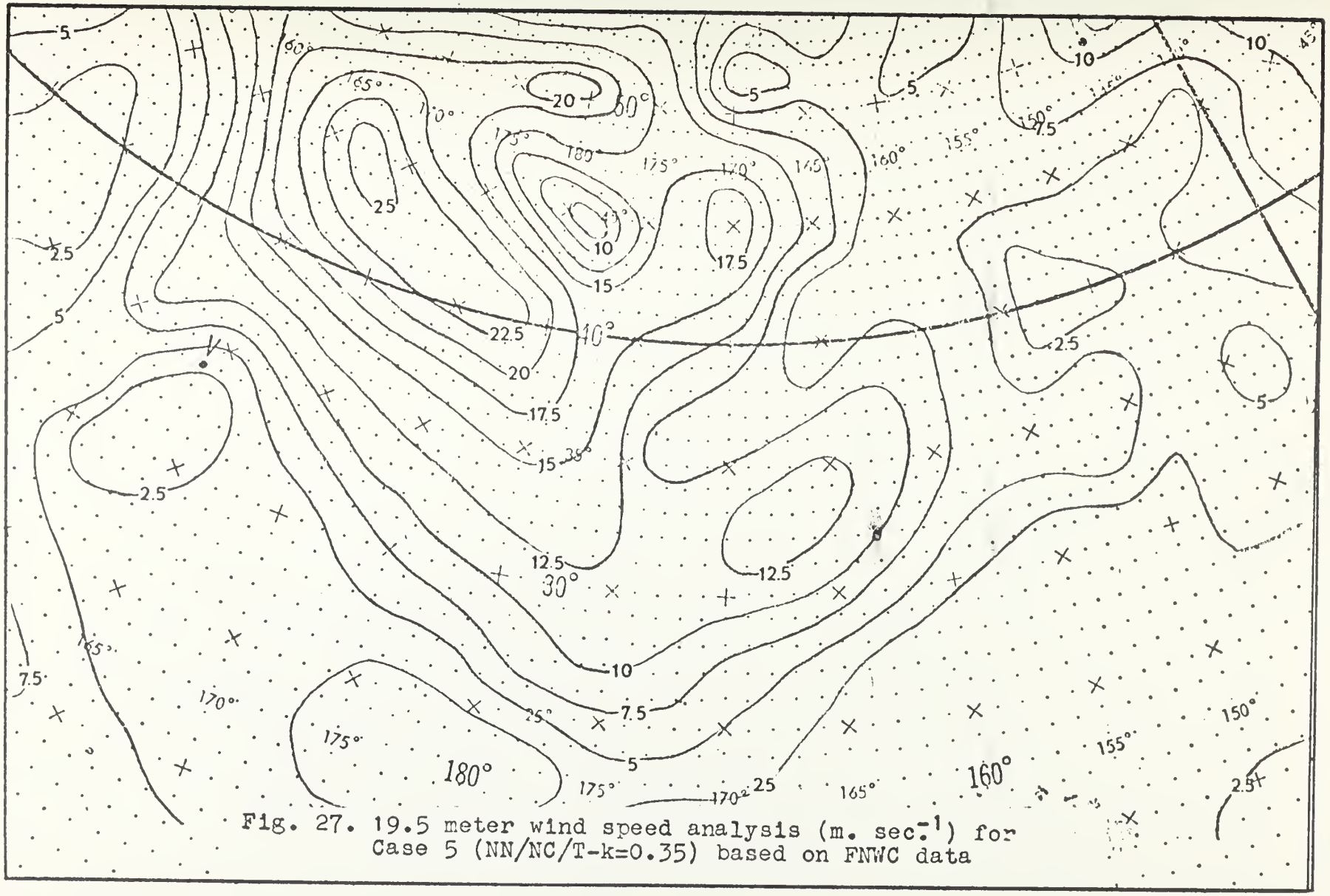

Fig. 27. 19.5 meter wind speed analysis (m. sec.$^{-1}$) for Case 5 (NN/NC/T-k=0.35) based on FNWC data

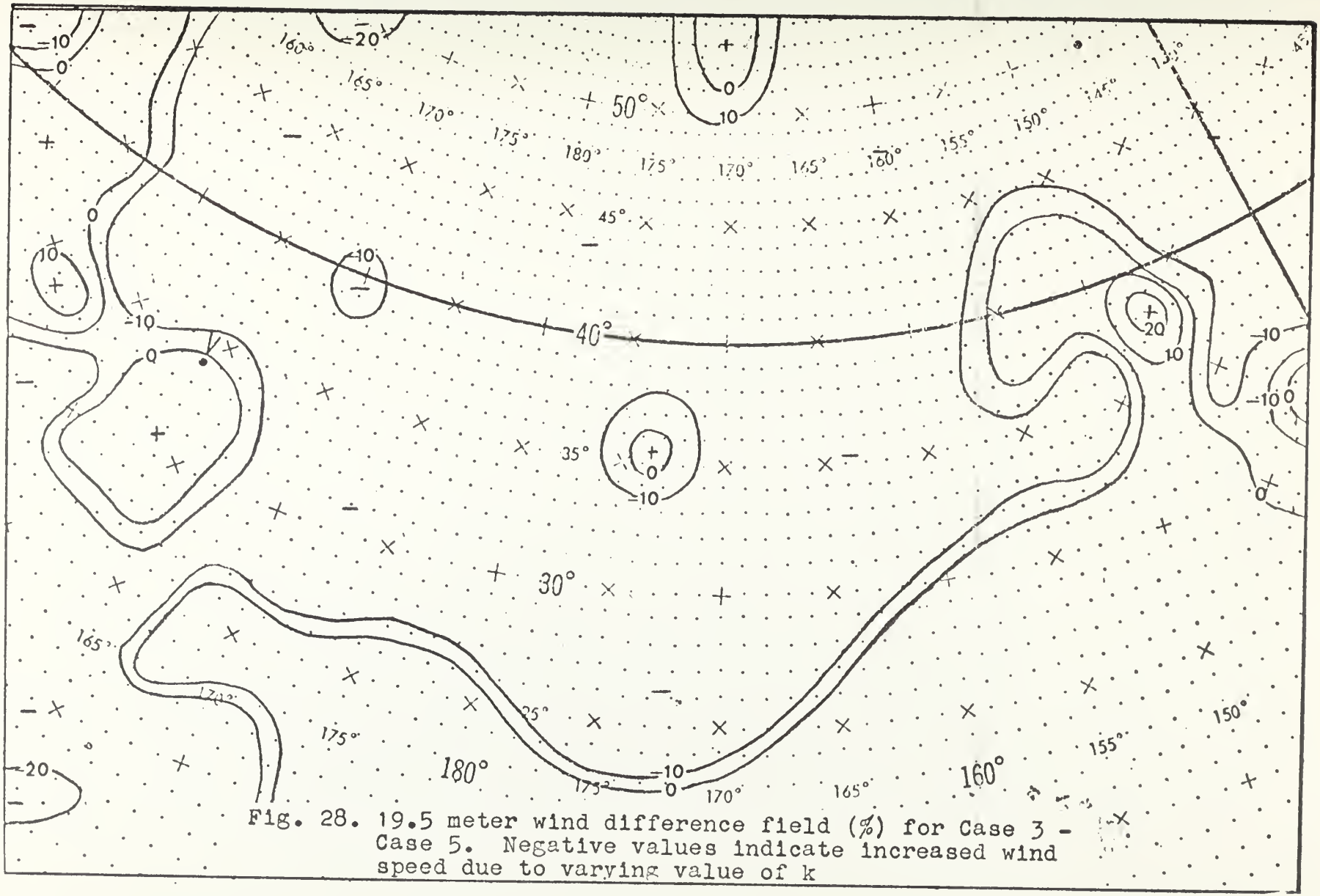

Fig. 28. 19.5 meter wind difference field (%) for Case 3 - Case 5. Negative values indicate increased wind speed due to varying value of k

discrepancies noted by Businger et al.. Because the von Kármán constant appears in several expressions in the boundary layer model, the importance of its change in the two-layer model was not known. These results indicate that the difference between $k = 0.35$ and $k = 0.40$ is important.

In summary, the five cases described above indicate which terms were most influential in the model. It should be remembered that most of the subtropical points were not influenced by the model since the wind speeds were generally less than 5.0 meters/second. Of all the modifications to the model, the curvature correction to the external field produced the largest variation over the entire grid. Changing k from 0.40 to 0.35 accounted for the second most significant change. Differences in the surface wind fields were evident, however, when specifications in the model were made. Of the two possible specifications, stability appeared to be more significant than the thermal wind with respect to area influenced and per cent difference changes.

Although the influence of the thermal wind in this model appears to be small with respect to the relative magnitude of the computed wind, the influence it has on the direction of the wind appears to be significant. The difference field, in degrees, of the wind direction for NN/NC/T - NN/NC/NT appears in Figure 29. This field represents the difference in wind direction between a case with and a case without the thermal wind specification. The region of significant differences does not coincide with that region where the thermal wind effect was large

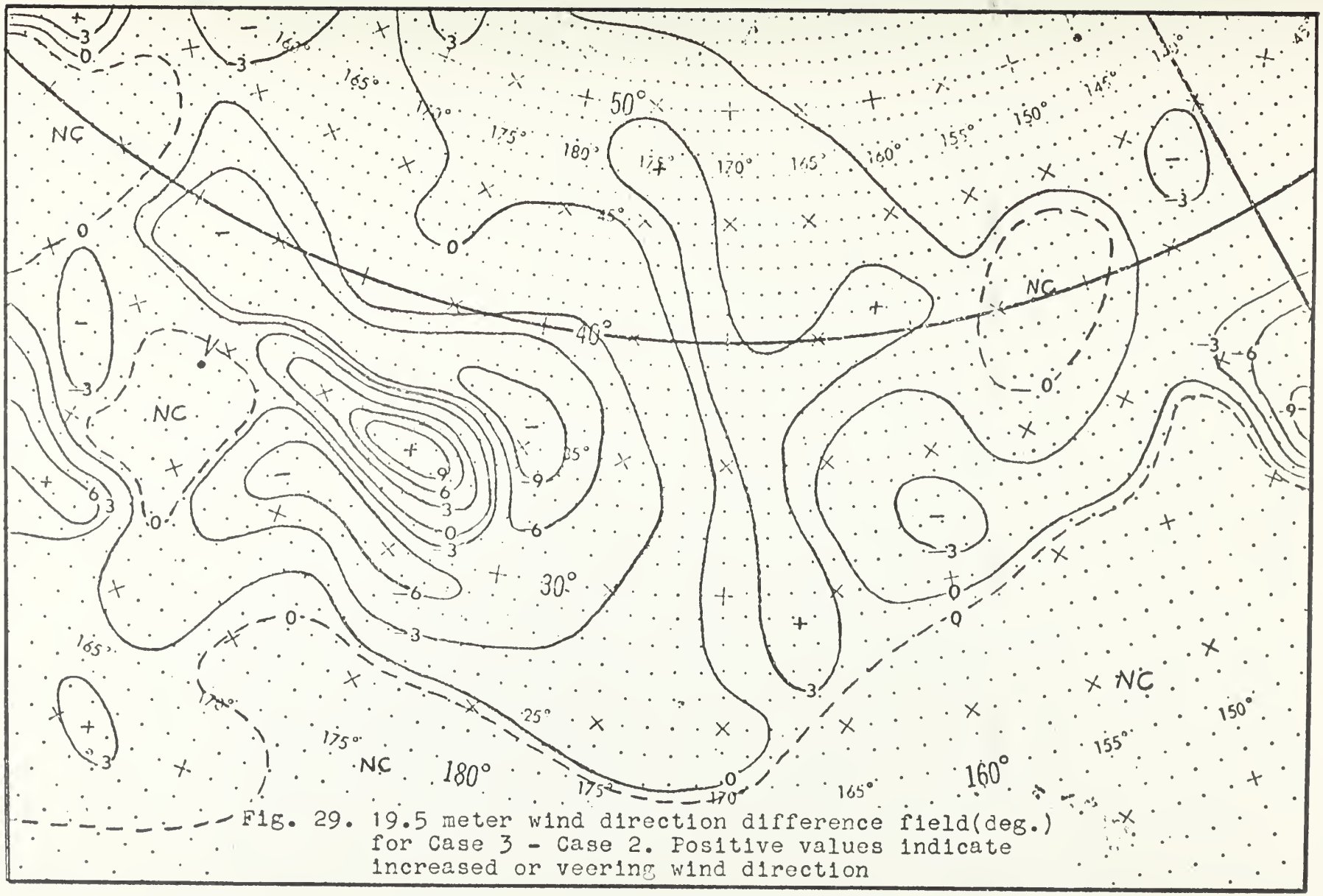

Fig. 29. 19.5 meter wind direction difference field(deg.) for Case 3 - Case 2. Positive values indicate increased or veering wind direction

with respect to wind speed. Positive values in Figure 29 correspond to a veering wind and negative values correspond to a backing wind. It is noted that the direction change due to baroclinicity is primarily determined by the angle between the thermal and geostrophic winds.

C. COMPARISONS OF COMPUTED WINDS WITH OBSERVED WINDS

These comparisons will be described for the case NN/C/T with $k = 0.35$. The 19.5 meter wind fields computed from the other cases were compared to the subjectively analyzed observed surface wind field (Figure 30) and in all cases the computed winds underestimate the observed winds. This was also the case when the above corrections were included, but yielded the best results with respect to the magnitude and patterns of the wind speeds.

Because the previous comparisons revealed the importance of the specifications of the external wind field with respect to curvature, it was considered necessary in this comparison to examine the importance of the initial analysis (FNWC or subjective). The 19.5 meter wind field computed with the above specifications and with the FNWC analysis is shown in Figure 31 and the wind field based on subjective analysis is seen in Figure 32. The observed surface wind field which appears in Figure 30 was analyzed using only those observations reported above 10 meters/second. In Figures 31 and 32, the maximum contour, 30 meters/second, agrees with the observed maximum wind speed, but the objective analysis does not indicate the 25 meter/second maximum east of the low.

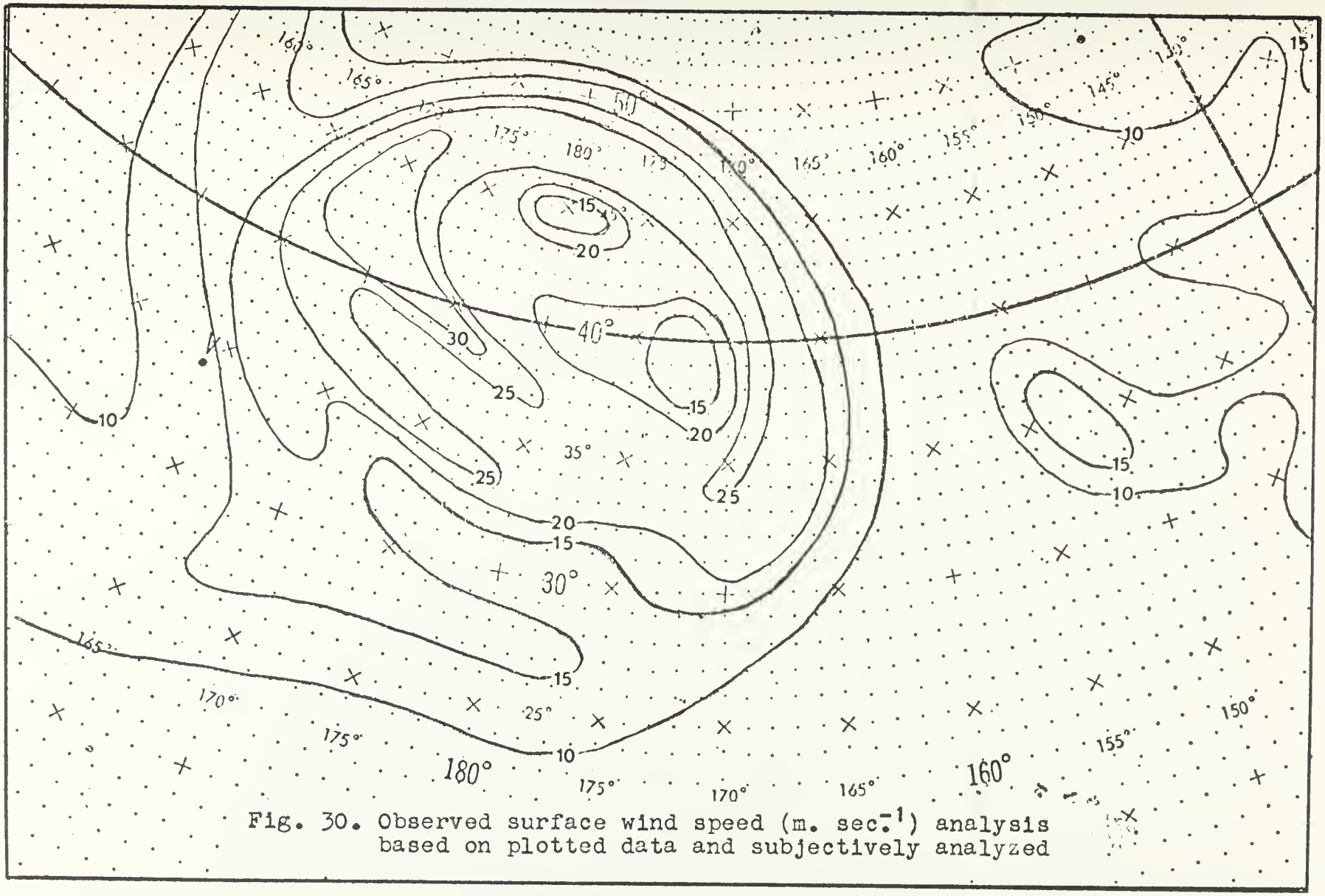

Fig. 30. Observed surface wind speed (m. sec.$^{-1}$) analysis based on plotted data and subjectively analyzed

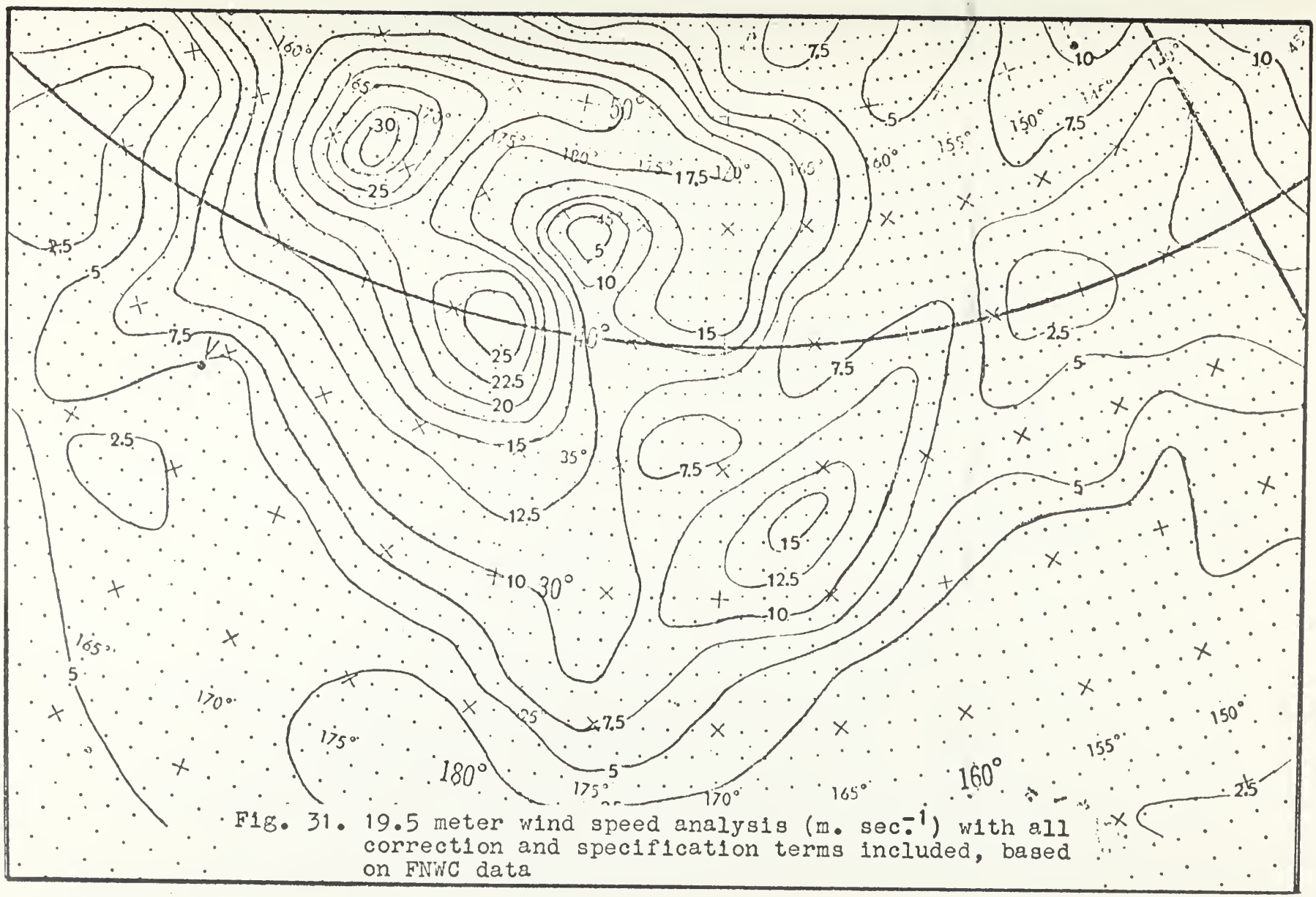

Fig. 31. 19.5 meter wind speed analysis (m. $sec.^{-1}$) with all correction and specification terms included, based on FNWC data

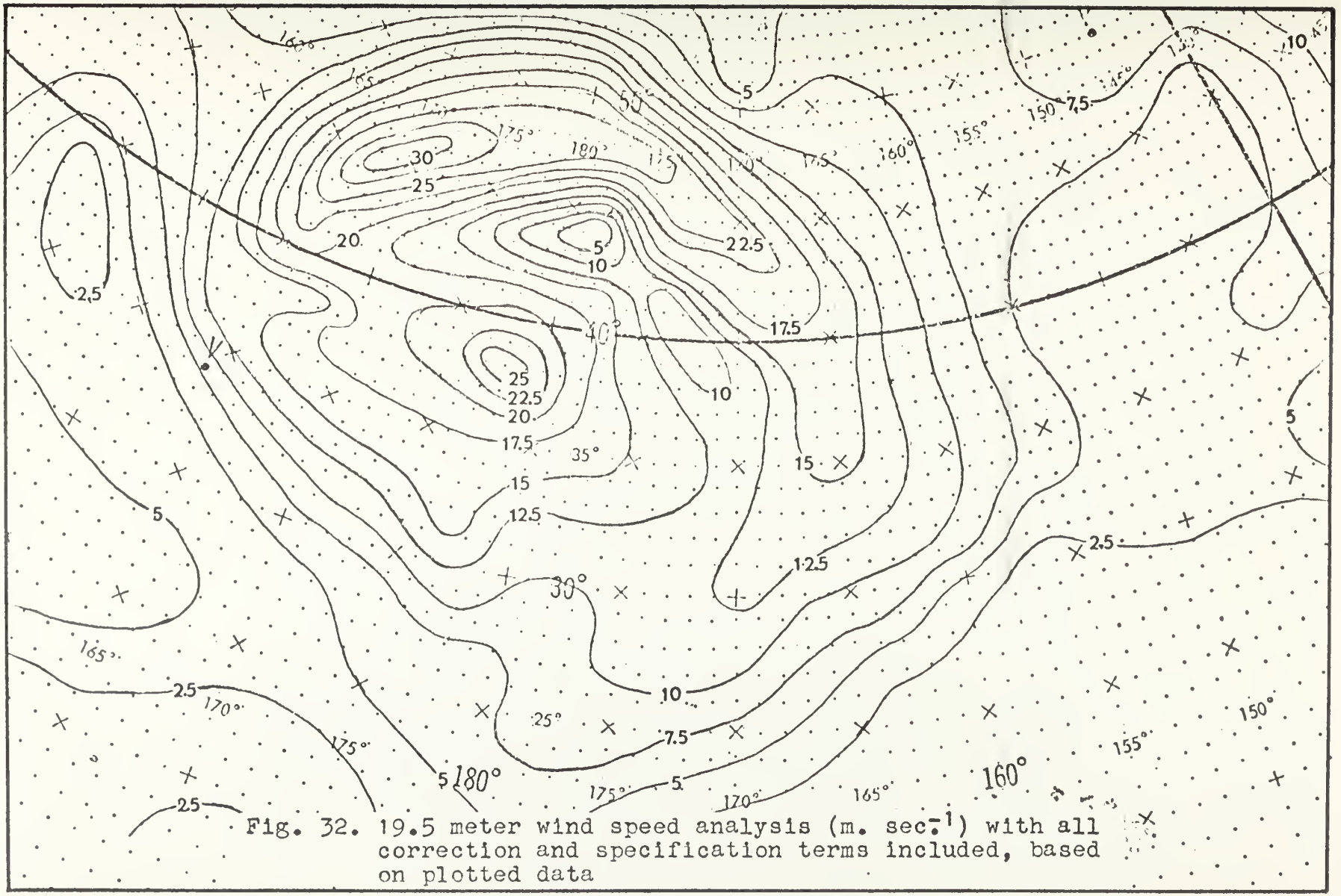

Fig. 32. 19.5 meter wind speed analysis (m. sec.$^{-1}$) with all correction and specification terms included, based on plotted data

A comparison of computed 19.5 meter winds from the two analyses (Figures 31 and 32) and the external wind fields (Figures 11 and 15) shows that differences in the external wind fields are consistently carried through the model. The model, however, was able to produce 19.5 meter wind fields in both cases which were in good agreement with the observed wind field, at least for wind speeds over 10 meters/second.

D. RESULTS FROM WAVE HEIGHT COMPUTATIONS

Wave height fields were computed using the 19.5 meter wind fields obtained from the boundary layer model and the simplified wave height program developed from the FNWC operational sea-swell model. The program was run starting at 00 GMT 28 Nov in order to build history for this analysis. The 19.5 meter wind computations were obtained using all specifications and corrections described previously, and they were also made on both the FNWC and subjectively analyzed fields. The computed wave field from the FNWC data is seen in Figure 33 and the wave field from the subjective analysis appears in Figure 34. The observed wave field obtained from synoptic observations is depicted in Figure 35. It is noted that wave height is probably the most difficult parameter to observe and therefore a representative analysis of the observed wave field is difficult to achieve.

The wave field obtained from the subjective analysis, Figure 34, appears to be in good agreement with the observed heights with maximum computed heights slightly less than the maximum observed heights.

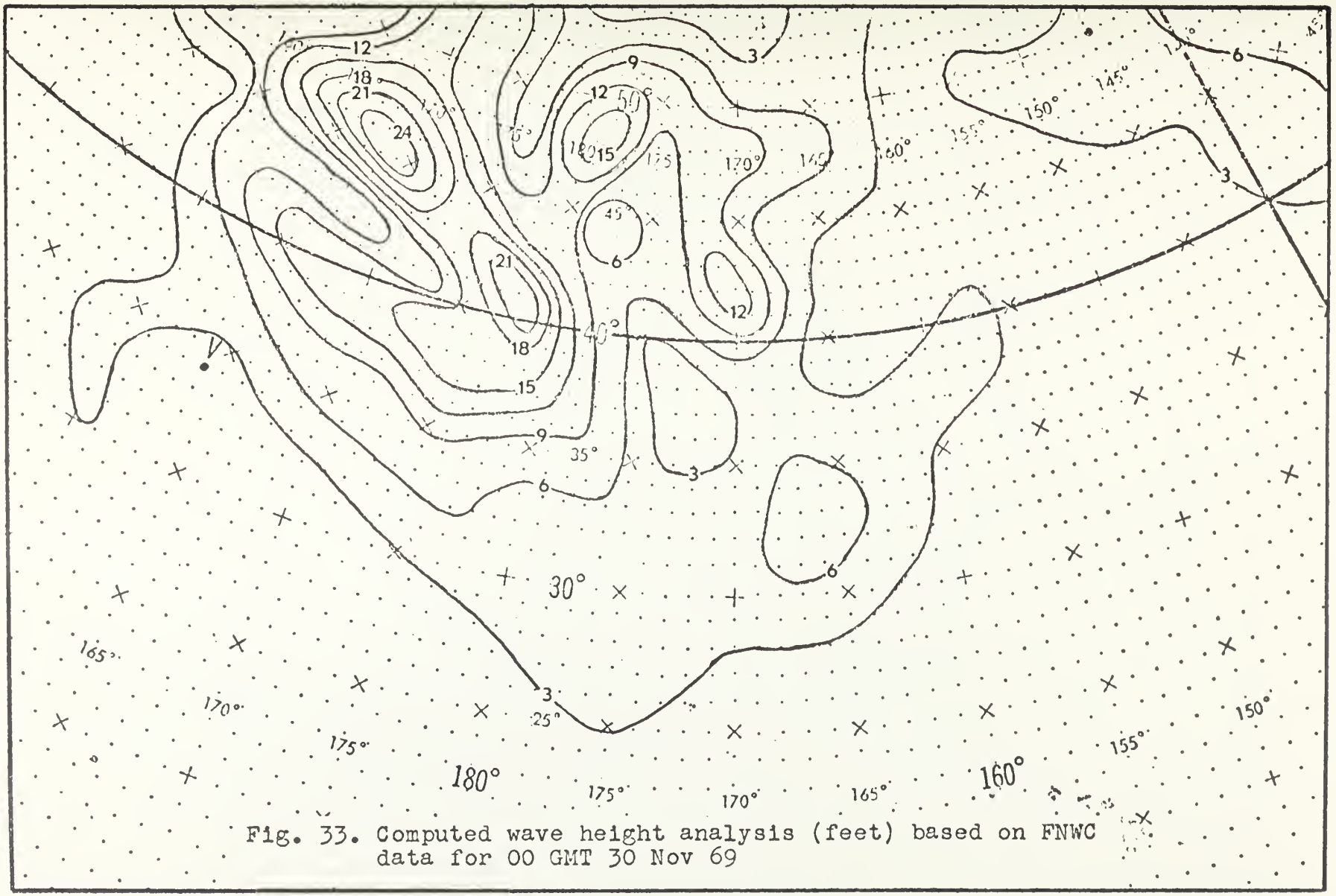

Fig. 33. Computed wave height analysis (feet) based on FNWC data for 00 GMT 30 Nov 69

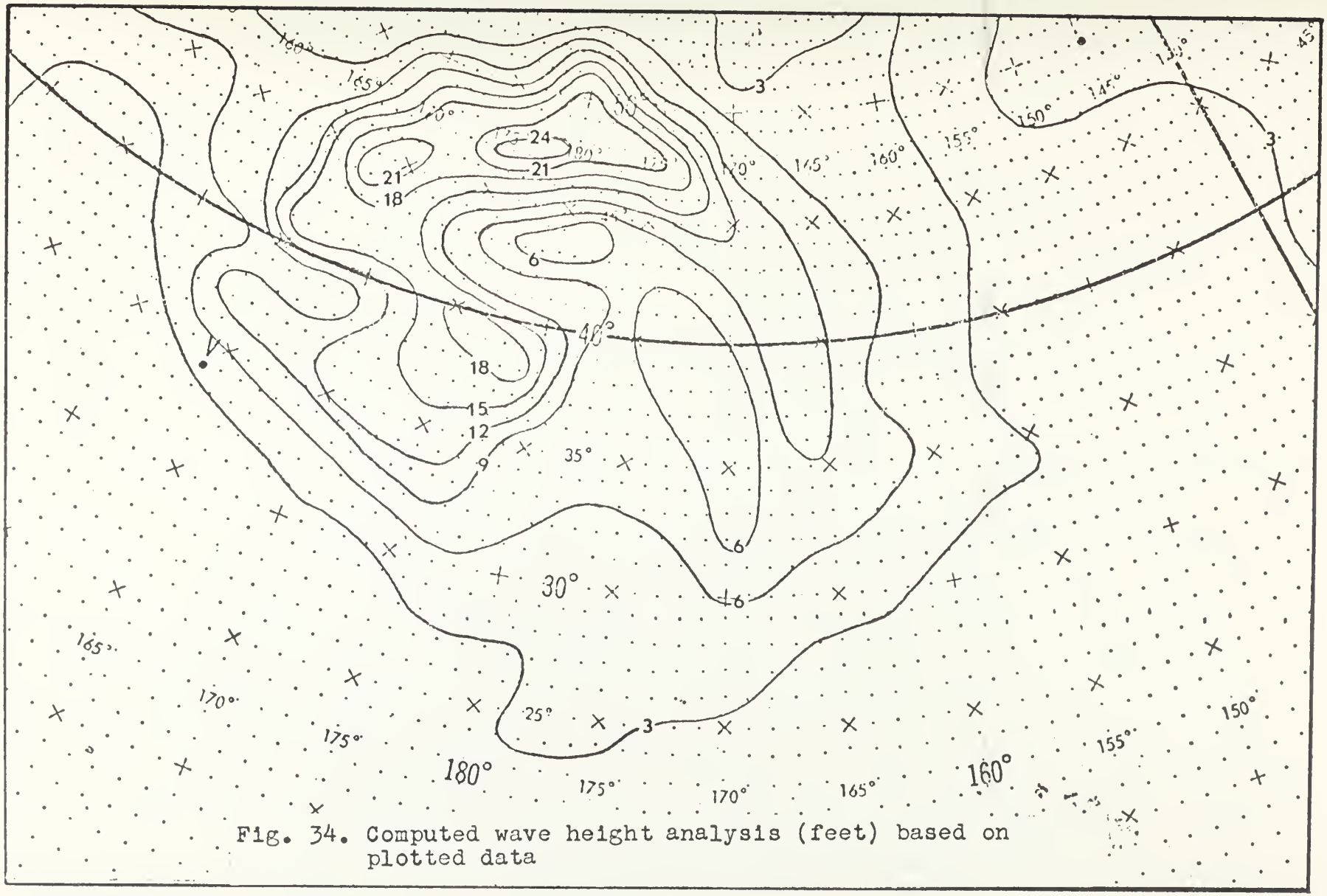

Fig. 34. Computed wave height analysis (feet) based on plotted data

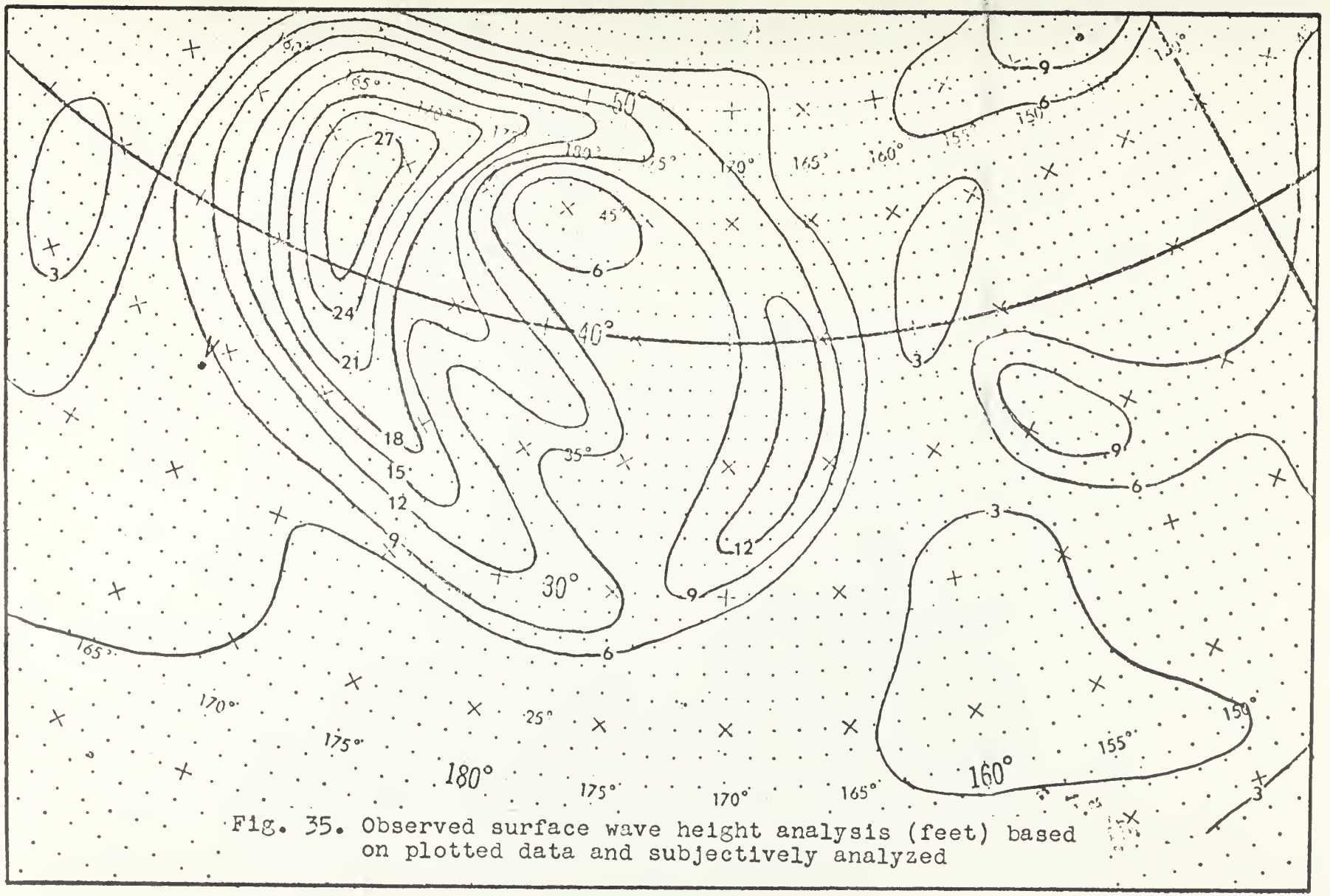

Fig. 35. Observed surface wave height analysis (feet) based on plotted data and subjectively analyzed

Results computed from the FNWC analysis, Figure 33, appear to have similar agreement with respect to the maximum height but poorer agreement with respect to the overall pattern of the wave field.

In general these results indicate that the two-layer model can produce surface wind fields which can be used for wave height analysis, even from a very simple wave model. It is noted that in the subtropics the wave heights computed from both sets of analysis are considerably below the observed wave heights. This is probably due to low surface geostrophic wind speeds in this area and the fact that no corrections are made for stability or baroclinicity at low wind speeds. This could possibly be corrected in the model by selecting a higher initial value for the drag coefficient.

E. RESULTS FROM INDEX OF REFRACTION COMPUTATIONS

A final application of the boundary layer model was the computation of the index of refraction structure constant (C_T^2) using (84). The ratio of the exchange coefficients was determined from (85) and the input data for this equation were obtained by including the stability effect, the thermal wind effect, the correction for curvature, and using $k = 0.35$. All parameters needed to compute C_T^2 were determined in the model.

The results from these computations appear in Figure 36. Values of C_T^2 range from 0.0 in regions of near neutral stratification to a maximum of 0.181 in the region of maximum wind speeds. Comparisons of

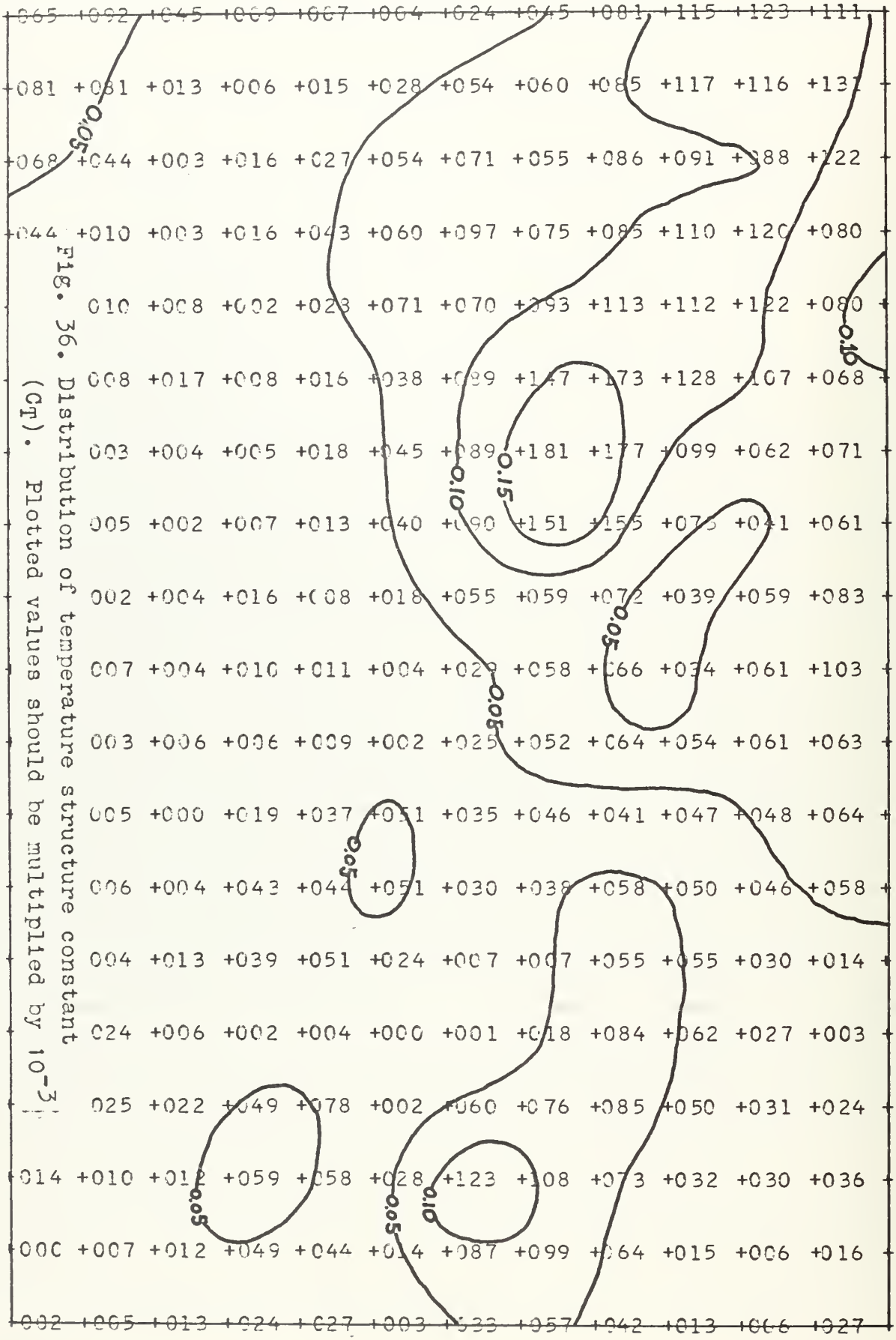

Fig. 36. Distribution of temperature structure constant (C_T). Plotted values should be multiplied by 10^{-3}.

these values with those measured by Portman et al. (1968) indicate that they are comparable in regions of low wind speed with $\theta_a - \theta_s$ less than 1 degree. Although no definite relation between C_T^2 and wind speed or $\theta_a - \theta_s$ appears in Figure 36, larger values of C_T^2 appear to be associated with the greater wind speeds and larger instability ($\theta_a - \theta_s$ ranging from -1 to -6°C).

The results indicate that a horizontal distribution of C_T^2 for a given height, in this case 19.5 meters, can be computed with the model with some degree of confidence in the range of values obtained. Comparisons should be made between results computed by this model and observations of C_T^2 to obtain better verification.

VI. CONCLUSIONS

The results of this study have indicated that a marine boundary layer model can be applied to synoptic scale data to obtain various surface parameters. These parameters include friction velocity (U_*), surface roughness (z_o), surface Rossby number (R_o), 19.5 meter wind ($U_{19.5}$), veering angle (Ψ_o), and stability length (z/L).

First, the results indicate that the curvature correction produced the greatest change to the wind analysis. However, stability and modification of the von Kármán constant produced significant changes in the field, while changes due to the thermal wind were confined primarily to changes in wind direction.

Second, the 19.5 meter wind was computed including various physical specifications and corrections and compared with synoptic observations. The results indicate that the computed wind was lower than the observed wind in all areas and for all cases, but the general patterns agreed well with observations.

Finally, it appears that Cardone's planetary boundary model provides a reasonable framework to specify those surface layer parameters required for spectral wave forecasting and index of refraction calculations.

Further studies are needed to more completely verify and improve the model. The specification of the drag coefficient is probably the aspect in this model which needs the most attention. The drag coefficient

has received considerable examination in observational investigations and the results indicate some disagreement among investigators. A suggestion of this study is to increase the initial value of C_z to increase the computed surface wind speeds especially in areas of low wind speed. Application of this model to a region of reliable synoptic data such as during the BOMEX experiment in 1969 would reduce some of the errors due to data input and also test the physics of the model in the tropical atmosphere. Finally, observations of the index of refraction over a wide range of wind speed and stability would allow reliable comparisons to be made of the structure constant (C_T).

```
C  PROGRAM TO COMPUTE A WIND AT 19.5 METERS USING BLACKADAR BAROCLINIC
C    MODEL OVER A SPECIFIED GRID
C
C     PACIFIC GRID: INPUT 21 X 15, OUTPUT 19 X 13 - INPUT (1,1)
C         CORRESPONDS TO FNWC (23,9) ON FORTRAN I,J GRID
C
C  DEFINITION OF PARAMETERS (UNITS OF MKS SYSTEM):
C    PRES = SURFACE PRESSURE (MBS) FOR GRID POINTS
C    TEMP = AIR TEMPERATURE (DEG C) FOR GRID POINTS
C    STEMP = SEA SURFACE TEMPERATURE (DEG C) FOR GRID POINTS
C    DIF = AIR TEMP - SEA TEMP (DEG C)
C    B = BLACKADAR CONSTANT
C    C1,C2,C3,B = CONSTANTS
C    D,S = DIRECTION AND SPEED OF GEOGRAPHIC WIND
C    ETAH = ANGLE BETWEEN GEOSTROPHIC WIND AND THERMAL WIND
C    F = CORIOLIS PARAMETER (/SEC)
C    FI = INTEGRATED PROFILE STABILITY PARAMETER
C    G = GEOSTROPHIC WIND (MPS)
C    GAN = GEOSTROPHIC WIND ANGLE
C    PARAM = MODIFIED STABILITY LENGTH (L')
C    PHI = INFLOW ANGLE
C    RHO = DENSITY OF AIR - COMPUTED FROM GAS EQUATION
C    ROSS = SFC ROSSBY NUMBER
C    SD = NON-DIMENSIONAL WIND SHEAR
C    TA = MEAN VIRTUAL TEMPERATURE = 280. DEG K
C    TAN = THERMAL WIND ANGLE
C    TH = NON-DIMENSIONAL THERMAL WIND
C    TORT = GRID SPACING(M)
C    VST = FRICTION VELOCITY (U STAR) (MPS)
C    W195 = 19.5 METER WIND (MPS)
C    W195U,W195V = COMPONENTS OF 19.5 METER WIND(MPS)
C    XK = VON KARMAN CONSTANT = 0.4
C    ZO = ROUGHNESS PARAMETER (M)
C    ZONL = DIMENSIONLESS STABILITY PARAMETER (L STAR)
C
      COMMON PRES(21,15),TEMP(21,15),DIF(21,15),W195U(21,15),W195V(21,15
     1),STEMP(21,15),W195(21,15),D(21,15),S(21,15),UGO(21,15),VGO(21,15)
      READ(5,990) I1,J1
    1 READ(5,1000,END=999)  ((PRES(I,J),I=1,I1),J=1,J1)
      READ(5,1000) ((TEMP(I,J),I=1,I1),J=1,J1)
      READ(5,1000) ((STEMP(I,J),I=1,I1),J=1,J1)
      DO 5 J=1,J1
      DO 5 I=1,I1
    5 DIF(I,J) = TEMP(I,J) - STEMP(I,J)
      CALL WNDY63
  999 STOP
 1000 FORMAT(13F6.1)
      END
```

```
      SUBROUTINE WNDY63
C
C  THE FOLLOWING CONDITIONS MAY BE SET IN THE SUBROUTINE:
C   NEUTRAL CONDITIONS - SET TD=0.0
C   NO CURVATURE CORRECTION - SET CURVE = 0.0
C   CURVATURE CORRECTION - SET CURVE = 1.0
C   NO THERMAL WIND CORRECTION - SET THERM = 0.0
C   COMPUTE GRIDPOINT PARAMETERS AND INITIAL 19.5 METER WIND COMPONENTS
C   T2 IS DATE TIME GROUP (16 CHARACTERS)
C   T3 IS DESCRIPTION OF RUN (48 CHARACTERS)
C
      COMMON PRES(21,15),TEMP(21,15),DIF(21,15),W195U(21,15),W195V(21,15
     1),STEMP(21,15),W195(21,15),D(21,15),S(21,15),UGO(21,15),VGO(21,15)
      DIMENSION T2(4),T3(12),CT(21,15)
      C1 = 6.84E-05
      C2 = 4.28E-03
      C3 = -4.43E-04
      B = 3.0E-04
      BB = 0.81
      TA = 280.
      XK = 0.35
      GRAV = 9.8
      OMEGA = 7.292E-05
      RADIAN = 3.14159/180.
      READ(5,900) T2,T3
      WRITE(6,1000) T2,T3
      RR = 2.87E+06*1.0E-04
      DELTA = 3.81E05
      DO 400 J=2,14
      DO 400 I=2,20
      I1 = I+22
      J1 = J + 8
      RSQR = (I1-32)**2 + (J1-32)**2
      SINPHI = (973.752 - RSQR)/(973.752 + RSQR)
      F = 2.*OMEGA*SINPHI
      XM = 1.8666667/(1. + SINPHI)
      TORT = 1./(2.*DELTA*XM)
C
C   SET F = CONSTANT FOR LE 15 DEG LAT
C
      FTEST  = SIN(15.*RADIAN)
      IF(SINPHI.LT.FTEST)  F = 2.*OMEGA*FTEST
      THERM = (GRAV*TORT)/(F**2*(TEMP(I,J)+273.))
      RHO = PRES(I,J)/(RR*(TEMP(I,J)+273.))
      TD = DIF(I,J)
C
```

```
C  COMPUTE GEOSTROPHIC WIND FROM SFC P FIELD
C
      UGO(I,J) = -(TORT/(RHO*F))*(PRES(I,J+1) - PRES(I,J-1))
      VGO(I,J) = (TORT/(RHO*F))*(PRES(I+1,J) - PRES(I-1,J))
      G = SQRT(UGO(I,J)**2 + VGO(I,J)**2)
      CURVE = 0.0
      IF(CURVE.NE.1.0) GO TO 10
      IF(G.LE.0.0) GO TO 10
      CALL GRADWD(DELTA,XM,F,G,I,J)
      G = SQRT(UGO(I,J)**2 + VGO(I,J)**2)
   10 ZONL = 0.
      RICH = 0.
C
C  COMPUTE THERMAL WIND
C
      TXO =-THERM*(TEMP(I,J+1)-TEMP(I,J-1))
      TYO = THERM*(TEMP(I+1,J)-TEMP(I-1,J))
      TH = SQRT(TXO**2 +TYO**2)
      IF(TH.GT.100.) TH = 100.
      CALL VANG(UGO(I,J),VGO(I,J),GAN)
      CALL VANG(TXO,TYO,TAN)
  200 ETAH = TAN-GAN
  210 IF(G.GT. 5.0) GO TO 220
C
C  FOR WIND SPEED LESS THAN 5.0 METERS/SEC,BYPASS BLACKADAR BAROCLINIC MODEL
C       CONSTANT DRAG COEFFICIENT = 0.0220, CONSTANT INFLOW ANGLE = 15 DEG
C        19.5 METER WIND = 0.7 GEOSTROPHIC WIND
C
      VST = .0220 * G
      ZO =-C3
      PHI = 15.*RADIAN
      W195(I,J) = 0.7*G
      IF(G.LE.0.0) GO TO 215
      ZO = C1/VST + C2*VST**2 + C3
  215 FE = 0.0
      PARAM = 0.0
      SD = 1.0
      GO TO 340
C
C  INITIALIZE BAROCLINIC MODEL
C
  220 VST = 0.0245 * G
      T = 0.0
      ETA = 0.0
      INDEX = 1
      IF(TD.GT.4.) TD = 4.0
      IF(TD.LT.-15.)  TD = -15.
      IF(ABS(TD).GT.1.0) GO TO 230
```

```
C
CC    ABSOLUTE VALUE OF AIR-SEA TEMPERATURE DIFFERENCE LE 1.0
CC       CONSTANT DRAG COEFFICIENT = 0.0245
C
         ZONL = 0.0
         PARAM = 0.0
         FI = 0.0
         FE = 0.0
         SD = 1.0
         GO TO 250
C
CC     ABSOLUTE VALUE OF AIR-SEA TEMP DIFFERENCE GT 1.0
C
  230 PARAM = TA*VST**2/(.1*XK**2*GRAV*TD)
  240 ZONL = ((B*G)/F)/PARAM
      CALL PSI(ZONL,FI,RICH)
      CALL SHR(ZONL,SD,RICH)
C
CC START BLACKADAR BAROCLINIC MODEL
C
  250 ZO = C1/VST + C2*VST**2 + C3
      CPA = (B*G/(F*SD))*(ALOG(B*G/(F*ZO))-FI)
      BET = SQRT(SD*F**2/(2.*VST*XK*B*G))
      P = SQRT(1.+2.*CPA**2*BET**2+2.*CPA*BET)
      R = SQRT(1.+(F**2*T**2*CPA**2)/G**2-(2.*F*T*CPA*COS(ETA))/G)
      ALPH = ARSIN(CPA*BET/P)
      ARGUM = (F*T*CPA*SIN(ETA)/(R*G))
      GAMMA = ARSIN(ARGUM)
      PHI = ATAN(SIN(ALPH+GAMMA)/(P/R-COS(ALPH+GAMMA)))
      VSTN = ((0.4*G*R*SIN(ALPH+GAMMA))/(P*SIN(PHI)))/(ALOG(B*G/(F*ZO))-
     1FI)
      TEST = ABS(VSTN-VST)
      IF((TEST - 0.05).LE.0.0) GO TO 270
  260 VST = VSTN
      GO TO 250
  270 IF(ZONL-0.) 280,290,280
  280 AA = 10./PARAM
      CALL PSI(AA,FE,RICH)
      ZO = C1/VST + C2*VST**2 + C3
      PARMNU =(VST**2*TA*(ALOG(10./ZO)-FE))/(XK**2*GRAV*TD)
      IF(ABS(PARMNU-PARAM).LT.5.) GO TO 290
      PARAM = PARMNU
      GO TO 240
  290 IF(INDEX-2) 300,310,300
  300 T = TH
      ETA = ETAH
      INDEX = 2
      GO TO 250
```

```
  310 IF(PARAM.NE.0.) GO TO 320
      ANEM = 0.
      ZONL = 0.0
      GO TO 330
  320 ZONL = 19.5/PARAM
      CALL PSI(ZONL,ANEM,RICH)
  330 W195(I,J) = (VST/XK)*(ALOG(19.5/ZO)-ANEM)
  340 PHIDEG = PHI/0.01745
      W195U(I,J) = W195(I,J)*(COS(GAN+PHI))
      W195V(I,J) = W195(I,J)*(SIN(GAN+PHI))
      IF(G.LE.0.0) GO TO 342
      ROSS = G/(F*ZO)
      ROSLOG = ALOG10(ROSS)
      USTARG = VST/G
      RATIO = W195(I,J)/G
      GO TO 345
  342 ROSLOG = 0.0
      USTARG =99.999
      RATIO = 99.99
C
C  CALCULATE INDEX OF REFRACTION (CT)
C
  345 ZHT = 19.5
      IF(PARAM.NE.0.0) GO TO 350
      ZL = 0.0
      XKHKM = 1.0
      GO TO 360
  350 ZL = ZHT/PARAM
      IF(ZL.LE.0.06) GO TO 355
      XKHKM = 1.0
      GO TO 360
  355 XKHKM = 1.35*(SQRT(1. - 9.*ZL)/((1. - 15.*ZL)**0.25))
  360 DTDZ = (SD*TD)/(ZHT*(ALOG(10./ZO)-FE))
      CT11 =(XK*ZHT)**1.3333333
      CT22 = (SD-ZL)**0.3333333
      CT(I,J) =SQRT ((BB*XKHKM*CT11*DTDZ**2)/(SD*CT22))
      WRITE(6,1100) I,J,DIF(I,J),G,ZO,ZONL,PHIDEG,VST,W195(I,J),ROSLOG,
     1USTARG,XKHKM,CT(I,J),RICH
  400 CONTINUE
      RETURN
  900 FORMAT(4A4/12A4)
 1000 FORMAT('1',2X,'OUTPUT FOR ',4A4,2X,12A4//' I',3X,
     1'J',2X,'AIR-SEA DIF',2X,'GEOST WIND',2X,'ROUGH PARAM',3X,'Z/L',3
     2X,'PHI(DEG)',2X,'USTAR',2X,'W195',2X,'LOG ROSSBY NO',2X,'USTAR/G',
     32X,'ALPHA ',2X,'I OF REF',4X,'RI'///)
 1100 FORMAT(1X,I2,2X,I2,5X,F5.1,8X,F4.1,6X,F8.6,3X,F6.2,4X,F5.1,4X,F5.3
     1,2X,F4.1,7X,F4.2,6X,F6.4,4X,F4.2,4X,F5.3,3X,F7.3/)
      END
```

```
      SUBROUTINE PSI(P,B,C)
C
      IF(P.GT.0.) GO TO 10
      CALL SHR(P,S,D)
      B    = 1.-S-3.*ALOG(S)+2.*ALOG((1.+S)/2)+2.*ATAN(S)-1.5708+ALOG((1.
     1+S**2)/2.)
      C = D
      RETURN
   10 B=-7.*P
      C = P
      RETURN
      END


      SUBROUTINE SHR(PS,B,C)
C
      IF(PS.GT.0.) GO TO 30
      RI  = PS
   10 RINEW = PS*(1.0-18.*RI)**(1./4.)
      IF(ABS(RINEW-RI).LT.0.01 ) GO TO 20
      RI  = RINEW
      GO TO 10
   20 B    = 1./(1.-18.*RINEW)**(1./4.)
      C = RINEW
      RETURN
   30 B    = 1.+7.*PS
      C = PS
      RETURN
      END


      SUBROUTINE GRIDEG (I,J,DEGLAT,DEGLON)
C
C   SUBROUTINE TO COMPUTE LAT - LONG VALUES FROM FNWC I,J GRID
C   LONGITUDE IN DEGREES AND DECIMAL FRACTIONS, + WEST FROM 0 DEGREES.
C
      RE = 31.205**2
      YP = I - 32.
      XP = J - 32.
      DEGLAT = 57.2957795*ARSIN((RE-XP**2-YP**2)/(RE+XP**2+YP**2))
      IF(XP.NE.0.0) GO TO 20
  102 IF(YP) 103,104,105
  104 ANG = 0.
      GO TO 50
  103 ANG = 80.
      GO TO 50
```

```
  105 ANG = 260.
      GO TO 50
   20 ANG = 350. - ATAN2(YP,XP)*57.2957795
      IF(ANG.GE.0.0) GO TO 50
      ANG = 360. + ANG
   50 IF((ANG - 360.).LE.0.0) GO TO 55
      ANG = ANG - 360.
   55 DEGLON = ANG
      RETURN
      END

      SUBROUTINE GEOGV
C
CC    CALCULATE GEOGRAPHIC WIND DIR(D) AND SPEED(S) FROM U  AND V
CC         COMPONENTS OF WIND ON THE I,J GRID
C
      COMMON PRES(21,15),TEMP(21,15),DIF(21,15),W195U(21,15),W195V(21,15
     1),STEMP(21,15),W195(21,15),D(21,15),S(21,15),UGO(21,15),VGO(21,15)
      PI = 3.14159
      DO 10 J=2,14
      L = J + 8
      DO 10 I=2,20
      K = I + 22
      CALL GRIDEG(K,L,ALAT,ALON)
      AA = W195U(I,J)
      BB = W195V(I,J)
      CALL VANG(AA,BB,ANGLE)
      ANGLE = ANGLE*180./3.14159
      D(I,J) = ALON + ANGLE - 260.
      IF(D(I,J).LT.0.0)  D(I,J) = 360. + D(I,J)
      D(I,J) = AMOD(D(I,J),360.)
      S(I,J) = SQRT(W195U(I,J)**2 + W195V(I,J)**2)
   10 CONTINUE
      RETURN
      END

      SUBROUTINE VANG(A,B,ANGLE)
C
CC    COMPUTE ANGLE IN I,J COORDINATES: A,B ARE I,J COMPONENTS RESPECTIVELY,
CC         ANGLE IS COMPUTED ANGLE IN RADIANS
C
      IF(A.NE.0.0.AND.B.NE.0.0) GO TO 20
      IF(A.NE.0.0) GO TO 10
      ANGLE = 90.
      IF(B.LT.0.0) ANGLE = 270.
      IF(A.EQ.0.0.AND.B.EQ.0.0) ANGLE = 0.0
```

```
      GO TO 30
   10 ANGLE = 0.0
      IF(A.LT.0.0) ANGLE = 180.
      GO TO 30
   20 ANGLE = ATAN2(B,A)*180./3.14159
      IF(ANGLE.LT.0.0) ANGLE = 360.+ ANGLE
   30 ANGLE = ANGLE*3.14159/180.
      RETURN
      END


      SUBROUTINE GRADWD(A,B,C,E,I,J)
C
CCC   SUBROUTINE TO COMPUTE A GRADIENT WIND USING CURVATURE AND THE GEOSTROPHIC
C       WIND
C
      COMMON PRES(21,15),TEMP(21,15),DIF(21,15),W195U(21,15),W195V(21,15
     1),STEMP(21,15),W195(21,15),D(21,15),S(21,15),UGO(21,15),VGO(21,15)
      FMAX = 0.75
      FMIN = -3./16.
      DELTAM = A*B
      XCOS = UGO(I,J)/E
      XSIN = VGO(I,J)/E
      DPDX = (PRES(I+1,J) - PRES(I-1,J))/(2.0*DELTAM)
      DPDY = (PRES(I,J+1) - PRES(I,J-1))/(2.0*DELTAM)
      D2PDX = (PRES(I+1,J) - 2.*PRES(I,J) + PRES(I-1,J))/(DELTAM**2)
      D2PDY = (PRES(I,J+1) - 2.*PRES(I,J) + PRES(I,J-1))/(DELTAM**2)
      D2PDXY = (PRES(I+1,J+1) - PRES(I-1,J+1) - PRES(I+1,J-1) + PRES(I-1
     1,J-1)) /(4.*(DELTAM**2))
      IF(DPDY.EQ.0.0) GO TO 10
    5 ANUM = (DPDY**2)*SQRT((1.0 + (DPDX/DPDY)**2)**3)
      DENOM = DPDX*(2.*D2PDXY - D2PDY*(DPDX/DPDY)) - DPDY*D2PDX
    6 IF(DENOM.EQ.0.0) GO TO 10
      IF(ANUM.EQ.0.0) GO TO 10
      RCURV = ANUM/DENOM
      VGRF = E/(RCURV*C)
      IF(VGRF.LT.FMIN) VGRF = FMIN
      IF(VGRF.GT.FMAX) VGRF = FMAX
      ROOT = 1./(0.5 + SQRT(0.25+VGRF))
      E = E**ROOT
      UGO(I,J) = XCOS*E
      VGO(I,J) = XSIN*E
   10 RETURN
      END
```

BIBLIOGRAPHY

Blackadar, A. K., 1965a: A simplified two-layer model of the baroclinic neutral atmospheric boundary layer. Air Force Cambridge Research Laboratories Report 65-531, pp. 49-65.

Blackadar, A. K., 1965b: A single layered theory of the vertical distribution of wind and turbulence in a baroclinic neutral atmospheric boundary layer. Air Force Cambridge Research Laboratories Report 65-531, pp. 1-22.

Blackadar, A. K., and J. K. S. Ching, 1965: Wind distribution in a steady state planetary boundary layer of the atmosphere with upward turbulent heat flux. Air Force Cambridge Research Laboratories Report 65-531, pp. 23-48.

Boston, N. E., 1970: An investigation of high wave number temperature and velocity spectra in air. Doctoral Dissertation, University of British Columbia.

Bunting, D. C., 1968: Ship anemometer heights above mean water level. U. S. Naval Oceanographic Office, Report IR 68-74, Washington, D. C.

Busch, N. E., and H. A. Panofsky, 1968: Recent spectra of atmospheric turbulence. Quart. J. Roy. Meteor. Soc., 94, 400.

Businger, J. A., J. C. Wyngaard, U. Izumi, and E. F. Bradley, 1971: Flux-profile relationships in the atmospheric surface layer. J. Atmos. Sci., 28, 181-189.

Cardone, V. J., 1969: Specification of the wind distribution in the marine boundary layer for wave forecasting. New York University, School of Engineering and Science, Scientific Report GSL-TR69-1, University Heights, New York.

Carstensen, L. P., 1967: Some effects of air-sea temperature difference, latitude and other factors on surface wind-geostrophic wind ratio and deflection angle. Fleet Numerical Weather Central, Technical Note 29, Monterey, California.

Carnock, H., 1955: Wind stress on a water surface. Quart. J. Roy. Meteor. Soc., 81, 639.

Clark, R. H., 1970: Observational studies in the atmospheric boundary layer. Quart. J. Roy. Meteor.Soc., 96, 91-114.

Cressman, G. P., 1959: An operational objective analysis system. Mon. Wea. Rev., 87, 367-374.

Corrsin, S., 1951: On the spectrum of isotropic temperature fluctuations in an isotropic turbulence. J. Appl. Phys., 22, 469.

Davidson, K. L., and D. J. Portman, 1971: The influence of water waves on the adjacent airflow. Symposium on Air-Sea Interaction, XV General Assembly of JUGG, Moscow, USSR (unpublished).

Hinze, J. O., 1959: Turbulence. New York, McGraw Hill, 586 pp.

Hubert, W. E., and B. R. Mendenhall, 1970: The FNWC singular sea/swell model. Fleet Numerical Weather Central, Technical Note 59, Monterey, California.

Kraus, E. B., 1966: The aerodynamic roughness of the sea surface. J. Atmos. Sci., 23, 443-445.

Lettau, H. H., 1959: Wind profile, surface stress and geostrophic drag coefficients in the atmospheric surface layer. Advances in Geophysics, 6, 241-257.

Lumley, J. L., and H. A. Panofsky, 1964: The Structure of Atmospheric Turbulence. New York, Interscience Publishers, 231pp.

Mendenhall, B. R., 1967: A statistical study of friction wind veering in the planetary boundary layer. Dept. of Atmospheric Science, Colorado State University, Atmospheric Science Paper No. 116, Fort Collins, Colorado.

Panofsky, H. A., 1963: Determination of stress from wind and temperature measurements. Quart. J. Roy. Meteor. Soc., 88, 85-94.

Panofsky, H. A., 1968: The structure constant for the index of refraction in relation to the gradient of index of refraction in the surface layer. J. Geophys. Res., 73, 6047-6049.

Paulson, C. A., 1967: Profiles of wind speed, temperature, and humidity over the sea. Dept. of Atmospheric Sciences, Sci. Report NSF GP-2418, University of Washington, Seattle, Washington.

Paulson, C. A., 1970: The mathematical representation of wind speed and temperature profiles in the unstable atmospheric surface layer. J. Appl. Meteor., 9, 857-861.

Phelps, G. T. and S. Pond, 1971: Spectra of the temperature and humidity fluctuations and the fluxes of moisture and sensible heat in the marine boundary layer. J. Atmos. Sci., 28, 918-928.

Phillips, O. M., 1966: The Dynamics of the Upper Ocean. London, Cambridge University Press, 261 pp.

Portman, D. J., E. Ryznar, and A. A. Wagif, 1968: Laser scintillation caused by turbulence near the ground. U. S. Army Cold Regions Research and Engineering Laboratory, Research Report No. 225, Hanover, N. H.

Pushistov, P. Yu., 1970: The planetary atmospheric boundary layer in the equatorial region. Izv., Atmos. and Oceanic Phys., 6, 556-564.

Ruggles, K. W., 1970: The vertical mean wind profile over the ocean for light to moderate winds. J. Appl. Meteor., 9, 389-395.

Sheppard, P. A., 1958: Transfer across the Earth's surface and through the air above. Quart. J. Roy. Meteor. Soc., 84, 205-224.

Sheppard, P. A., 1969: The atmospheric boundary layer in relation to large-scale dynamics. Global Circulation of the Atmosphere. London, Salisbury Press.

Smith, S. D., 1967: Thrust anemometer measurements of wind-velocity spectra and of Reynolds stress over a coastal inlet. J. Marine Res., 25, 239-262.

Weiler, H. S., and R. W. Burling, 1967: Direct measurements of stress and spectra of turbulence in the boundary layer over the sea. J. Atmos. Sci., 24, 653-664.

INITIAL DISTRIBUTION LIST

		No. Copies
1.	Defense Documentation Cameron Station Alexandria, Virginia 22314	2
2.	Library, Code 0212 Naval Postgraduate School Monterey, California 93940	2
3.	Professor Kenneth Davidson, Code 51Ds Department of Meteorology Naval Postgraduate School Monterey, California 93940	5
4.	Professor Noel Boston, Code 58Bb Department of Oceanography Naval Postgraduate School Monterey, California 93940	1
5.	Lieutenant Donald R. McConathy Fleet Numerical Weather Central Monterey, California 93940	4
6.	Professor R. L. Haney Department of Meteorology Naval Postgraduate School Monterey, California 93940	1
7.	Department of Meteorology Naval Postgraduate School Monterey, California 93940	2
8.	Professor G. J. Haltiner Department of Meteorology Naval Postgraduate School Monterey, California 93940	1
9.	Professor R. L. Alberty Department of Meteorology Naval Postgraduate School Monterey, California 93940	1

10.	Professor R. L. Elsberry Department of Meteorology Naval Postgraduate School Monterey, California 93940	1
11.	Professor R. T. Williams Department of Meteorology Naval Postgraduate School Monterey, California 93940	1
12.	Naval Weather Service Command Naval Weather Service Command Headquarters Washington Navy Yard Washington, D. C. 20390	1
13.	Professor D. F. Leipper Department of Oceanography Naval Postgraduate School Monterey, California 93940	1
14.	Professor A. K. Blackadar Department of Meteorology Pennsylvania State University University Park, Pennsylvania 16802	1
15.	Professor H. A. Panofsky Department of Meteorology Pennsylvania State University University Park, Pennsylvania 16802	1
16.	Dr. Vincent J. Cardone School of Engineering and Science New York University University Heights, New York, N. Y. 10453	1
17.	Capt. W. E. Hubert, USN-Ret Fleet Numerical Weather Central Monterey, California 93940	1
18.	Dr. Jack Kaitala Fleet Numerical Weather Central Monterey, California 93940	1

Security Classification

DOCUMENT CONTROL DATA - R & D

(Security classification of title, body of abstract and indexing annotation must be entered when the overall report is classified)

1. ORIGINATING ACTIVITY *(Corporate author)*

Naval Postgraduate School
Monterey, California 93940

2a. REPORT SECURITY CLASSIFICATION

UNCLASSIFIED

2b. GROUP

3. REPORT TITLE

Specification of Marine Surface Boundary Layer Parameters

4. DESCRIPTIVE NOTES *(Type of report and, inclusive dates)*

Master's Thesis; March 1972

5. AUTHOR(S) *(First name, middle initial, last name)*

Donald Reed McConathy, Jr.

6. REPORT DATE	7a. TOTAL NO. OF PAGES	7b. NO. OF REFS
March 1972	105	33

8a. CONTRACT OR GRANT NO.	9a. ORIGINATOR'S REPORT NUMBER(S)
b. PROJECT NO.	
c.	9b. OTHER REPORT NO(S) *(Any other numbers that may be assigned this report)*
d.	

10. DISTRIBUTION STATEMENT

Approved for public release; distribution unlimited.

11. SUPPLEMENTARY NOTES	12. SPONSORING MILITARY ACTIVITY
	Naval Postgraduate School Monterey, California 93940

13. ABSTRACT

Specification of parameters defining the mean, as well as the turbulent properties, of the over water surface layer is examined. A baroclinic boundary layer model is considered using Cardone's modifications for the marine environment.

Data fields of pressure and temperature were selected as input, and original ship observations were utilized to verify the predicted surface parameters. The effects of stability changes, isobaric curvature, thermal wind, and the value of the von Karman constant in the model were examined with results shown.

Iteration criteria used in the model were evaluated with respect to operational application. Winds calculated by the model at the height of 19.5 meters were incorporated into the current FNWC wave height program, and the results compared with observed wave data. Turbulent parameters describing the properties of the index of refraction (C_n^2) were also computed and evaluated with respect to laser propagation criteria.

DD FORM 1 NOV 65 1473 (PAGE 1)

S/N 0101-807-6811

Security Classification

A-31408

KEY WORDS	LINK A		LINK B		LINK C	
	ROLE	WT	ROLE	WT	ROLE	WT
Baroclinic						
Barotropic						
Coriolis						
Layer						
Parameter						
Refraction						
Surface						
Wind						